Atmos. Chem. Phys., 26, 16683–16702, 2026
https://doi.org/10.5194/acp-26-16683-2026
© Author(s) 2026. This work is distributed under
the Creative Commons Attribution 4.0 License.

Atmospheric Chemistry and Physics
Open Access
EGU

Increasing and widespread deposition of trifluoroacetic acid from global emissions of HFO-1234yf in mobile-air conditioning

Lucy Hart[1], **Ryan Hossaini**[1], **Oliver Wild**[1], **Crispin Halsall**[1], **Martin K. Vollmer**[2], **and David Sherry**[3]

[1]Lancaster Environment Centre, Lancaster University, Lancaster, LA1 4YW, UK
[2]Laboratory for Air Pollution/Environmental Technology, Empa, Dübendorf, 8600, Switzerland
[3]Nolan Sherry & Associates (NSA), Surrey, UK

Correspondence: Lucy Hart (l.hart4@lancaster.ac.uk)

Received: 31 July 2026 – Discussion started: 7 August 2026
Revised: 7 November 2026 – Accepted: 9 November 2026 – Published: 23 November 2026

Abstract. HFO-1234yf is an emerging low global warming potential refrigerant with increasing emissions, especially from mobile air-conditioning (MACs), that are poorly constrained. It is oxidised in the atmosphere to form trifluoroacetic acid (TFA), a persistent, mobile, and widespread pollutant. Despite growing concerns around TFA accumulation in the environment, the contribution of HFO-1234yf to its global deposition is not known. Here, we present the first global bottom-up emissions inventory for HFO-1234yf from passenger vehicles. We use a chemical transport model to calculate the global TFA budget from these emissions and quantify source–receptor relationships from idealised emission scenarios. The magnitude and trend in HFO-1234yf emissions from North-West Europe are in close agreement with top-down assessments. Using our derived emissions, the model reproduces surface HFO-1234yf observations from the AGAGE network reasonably well. A sensitivity study using estimates of fugitive emissions from HFO-1234yf production improves agreement, particularly at Gosan, South Korea, where the model underestimates observations. We find that global TFA deposition from HFO-1234yf in MACs has increased from 0.078 (0.050–0.17) Gg yr^{-1} in 2014 to 3.5 (1.6-6.4) Gg yr^{-1} in 2024, with 75 % of cumulative HFO-1234yf emissions coming from Europe. A large proportion of TFA from HFO-1234yf (54 %) is deposited in oceans. Source–receptor analysis shows that most (86 %–97 %) TFA deposition occurs outside of the original HFO-1234yf emission region. All regions except Europe are net atmospheric importers of TFA, underscoring the importance of international efforts to reduce future TFA pollution.

1 Introduction

Hydrofluoroolefins (HFOs) are the latest generation of low global warming potential (GWP) and low ozone depleting refrigerants. Their use is increasing as they replace hydrofluorocarbons (HFCs) currently being phased down from production and consumption under the Kigali Amendment to the 1987 Montreal protocol. HFOs are structurally similar to HFCs but have a reactive double bond that reduces their atmospheric lifetime, and thus direct GWP (Salierno, 2024). However, experimental studies show that their atmospheric oxidation may result in the production of harmful degradation products, including the potent greenhouse gases HFC-23 and PFC-14 (e.g., McGillen et al., 2023; Pérez-Peña et al., 2023; Salierno, 2024; Sulbaek Andersen and Nielsen, 2022; Thomson et al., 2025; Van Hoomissen et al., 2025). Their quick removal from the atmosphere (within days to weeks), compared to HFCs (with lifetimes of years) also results in faster production of trifluoroacetic acid (TFA; CF_3COOH) – a highly persistent perfluoroalkyl substance (PFAS; OECD, 2021) which is the focus of this study.

TFA is a pollutant of emerging concern because of its high persistence and growing environmental concentrations (Arp et al., 2024). The science and policy around the risks of TFA to terrestrial and marine life are still evolving (Cousins et al., 2019; Neale et al., 2025), but the European Chemicals

Agency (ECHA) recently confirmed classification of TFA as toxic to reproduction, persistent, mobile, and toxic (ECHA, 2026). There are numerous sources of TFA to the environment, including fluorinated pesticides, pharmaceuticals, fluoropolymer burning, and industrial wastewater (Ellis et al., 2001; Joerss et al., 2024; Scheurer et al., 2017) but these are not well constrained. Atmospheric production of TFA from fluorinated refrigerant gases – namely hydrochlorofluorocarbons (HCFCs) and HFCs, is a major source (e.g., Hart et al., 2026; Pickard et al., 2020). These gases are globally well mixed, resulting in diffuse TFA production that is decoupled from emission sources, and their deposition footprint can reach remote regions including the poles (Pickard et al., 2020; Sanz Rodriguez et al., 2025). Based on chemical transport model (CTM) simulations that included an explicit treatment of atmospheric TFA production, our recent work showed that global TFA production from HCFCs and HFCs increased by a factor of 3.5 between 2000 (6.8 (5.9–7.6) Gg yr^{-1}) and 2022 (21.8 (18.6–25.0) Gg yr^{-1}) and that these sources alone can explain observed Arctic deposition trends over approximately the same period (Hart et al., 2026).

In contrast, TFA production from HFOs is less well constrained because of uncertainties in their emissions and degradation chemistry (e.g., Sulbaek Andersen et al., 2026). Several HFOs / HCFOs can be oxidised to TFA in the atmosphere (e.g., HFOs (1225zc, 1234yf, 1234ze(E/Z), 1234zf, 1336mzz(E/Z), 1345zfc, 1438mzz(E), 1447fz), and HCFO-1233zd(E/Z)) with TFA yields varying from $<7\,\%$ (HFO-1345zfc) to $\sim 100\,\%$ (HFO-1234yf; Sulbaek Andersen et al., 2026). Of these species, HFO-1234yf, HFO-1234ze(E), and HCFO-1233zd(E) are currently the most widely used (Vollmer et al., 2026a). This study focuses on HFO-1234yf because of its high TFA yield and potential to influence TFA deposition.

A number of modelling studies have examined the impact of replacing HFC-134a with HFO-1234yf in the mobile air conditioning (MAC) sector (David et al., 2021; Holland et al., 2021; Kazil et al., 2014; Luecken et al., 2010; Wang et al., 2024) and it is well established that TFA production from HFO-1234yf is concentrated closer to emission sources than from HFC-134a (Hart et al., 2026; Holland et al., 2021). Nevertheless, with a lifetime of the order of weeks, HFO-1234yf can also undergo long range transport before TFA is produced and deposited (e.g., Henne et al., 2012; Wang et al., 2024) and the impact of foreign emissions on low-emitting regions remains poorly quantified.

A recent study modelled TFA production from both the OH ($\sim 97\,\%$ of global HFO loss) and O_3 ($\sim 3\,\%$ loss) initiated oxidation of 15 HFOs (Khan et al., 2026). They examined the impact of idealised HFO-1234yf emissions from Europe, North America and Asia on within-region TFA deposition and found that 32 %, 31 %, and 30 % of TFA, respectively, was deposited within the emissions region. Given the potential for emissions from growing economies in Asia and the Global South to increase in the future (Wang et al., 2026) and the increasing use of HFOs beyond MACs (e.g., stationary refrigeration, foam blowing, aerosol propellants and solvents), there is a need to quantify the source-receptor (SR) relationships. SR relationships describe how emissions of HFO-1234yf from a source region i impact TFA deposition in region j. This can be a useful tool for policy makers to target policy at the most impactful regions and allows identification of regions that are most vulnerable to future TFA deposition.

Here, we present the first global bottom-up emission inventory of HFO-1234yf in passenger vehicle MACs from 2013–2024 and an estimate of fugitive emissions of HFO-1234yf from its production in 2024. We use a CTM to quantify TFA deposition from these emissions and compare the magnitude and spatial distribution of TFA production to that from HCFCs and HFCs. We also determine SR functions that relate HFO-1234yf emissions and TFA deposition in specified source and receptor regions, examine the impact of interannual variability in meteorological conditions on TFA deposition, and test the sensitivity of modelled TFA deposition to key uncertainties in the model parameterisation of its production and deposition.

The paper is structured as follows. Section 2 details the bottom-up approach used to calculate HFO-1234yf emissions from the MAC sector and leakage from production. Section 3 describes the CTM used and the model experiments that were performed to quantify TFA deposition and SR relationships. Our main results are presented in Sect. 4, including evaluation of our HFO-1234yf emissions against a recent top-down estimate (Sect. 4.1), findings from the SR analysis (Sect. 5), discussion of the implications of the SR analysis (Sects. 5.1 and 2), and uncertainty analysis of SR relationships (Sect. 5.3). A summary and concluding remarks are given in Sect. 6.

2 Bottom-up Modelling of Emissions

2.1 IPCC Tier 2a Methodology

Global HFO-1234yf emissions from passenger vehicle MAC systems were calculated annually by country from 2013–2024 using the IPCC Tier 2a bottom-up approach (IPCC, 2006). This emission factor method calculates total refrigerant emissions (E_{total}) from four lifecycle stages that include charging new equipment, operation and servicing, end-of-life disposal, and container management (Eq. 1).

$$E_{\text{total}} = E_{\text{charge}} + E_{\text{lifetime}} + E_{\text{end-of-life}} + E_{\text{container}} \quad (1)$$

Here, E_{charge}, E_{lifetime}, $E_{\text{end-of-life}}$, and $E_{\text{container}}$ represent refrigerant emissions from first fill, operation, end-of-life disposal, and containers, respectively. Each term in Eq. (1) is determined by multiplying the mass of refrigerant associated with each lifecycle stage by an emission factor (presented in Table 1), using the data and assumptions outlined below.

Table 1. Emission factors used in the bottom-up modelling of HFO-1234yf emissions.

	Non-Article 5 Countries	Article 5 (Groups 1 and 2) Countries	Source
EF_{can} (% yr^{-1})	20	20	IPCC (2006)
EF_{cyl} (% yr^{-1})	2	2	IPCC (2006)
EF_{FF} (% yr^{-1})	0.2	0.5	IPCC (2006)
EF_{OP} (% yr^{-1})	4 (2–6)	4 (2–6)	Our estimate
Recovery Efficiency (%)	50	0	IPCC (2006)
η_{res}	100 – EF_{OP}	100 – EF_{OP}	IPCC (2006)
x (%)	98	98	Our estimate

2.2 Charging Emissions

The charging emissions term (Eq. 2) represents emissions that occur during the charging of new equipment in the country where the vehicle was produced.

$$E_{\text{charge},t,c} = M_{t,c} \cdot EF_{FF} \tag{2}$$

where $M_{t,c}$ represents the mass of refrigerant charged into new equipment in the country of production (see Eq. 3), and EF_{FF} is the emission factor representing leakage during charging into new equipment (%). Subscripts t, and c represent the year and country.

$$M_{t,c} = N \cdot \text{charge} \cdot P_{t,c} \tag{3}$$

where N is the number of vehicles produced, charge is the average mass (g) of refrigerant in an individual MAC unit, and P (market penetration) represents the market fraction of HFC-134a substituted by HFO-1234yf. Data for car production and sales by country was sourced from the International Organisation of Motor Vehicle Manufacturers (OICA, 2025).

We conducted a market survey to determine the average nominal charge of refrigerant in passenger cars. Sales of new passenger vehicles were divided into six categories based on their European New Car Assessment Programme (NCAP) class: Small (A + B), Lower Medium (C), Upper Medium (D), Luxury (E + F), Multi-Purpose Vehicle, and Sports Utility Vehicle. Data was available on refrigerant charge by model (Database26, 2025) and we calculated the average charge weighted by the distribution of passenger cars sold across the above NCAP classes in Europe in 2023 (ACEA, 2025). Note that HFO-1234yf is also used in light-duty commercial vehicles in Europe as required by the European Directive 2006/40/EC (European Parliament and Council, 2006) but this sector is small in comparison to passenger cars (e.g., 2 % of emissions in Germany for 2024 (Warncke and Gschrey, 2026)). Given the small emissions from commercial vehicles and absence of regulation governing the transition to HFO-1234yf in heavy duty vehicles and trains, this inventory was restricted to passenger cars.

Following the approach of (Kish, 1995), the margin of error (E) at the 90 % confidence level was calculated to be 25 % using the equation:

$$E^2 = \frac{Z^2 \cdot \sigma^2 \cdot \text{Deff}}{n} \tag{4}$$

where $Z = 1.65$ is the critical value for a 90 % confidence level, $\sigma = 133$ is the standard deviation, Deff = 2.40 is the design effect, and $n = 288$ is the sample size. The design effect for unequal weights accounts for increased variance that arises when disproportionate allocation of samples across classes reduces the effective sample size. It is calculated as $1 + CV^2$, where CV is the coefficient of variation of the weights (Kish, 1995) and the effective sample size is n/Deff. The average charge (weighted average ± 25 %) of HFO-1234yf in European vehicles for the year 2023 was calculated to be 539 (457–620) g. This is within range of the HFC charge (400–800 g for 1990–2023) assumed in previous bottom-up modelling of emissions from MAC systems in light duty vehicles (UK National Inventory Document; UNFCCC, 2025) and the central value is similar to the 550 g adopted in earlier bottom-up studies (Papasavva et al., 2009; Henne et al., 2012). Data on passenger vehicle sales by class were not available at a global level so the European sales-weighted average charge was applied globally.

To determine the market penetration, we assumed a gradual uptake of HFO-1234yf up to complete substitution on the effective date of the regulation, then full regulatory compliance for countries with regulation on the phase-out of HFCs in MACs (EU, EFTA, UK, USA, Canada, and Japan). Data on the uptake of HFO-1234yf in MACs was available for Australia (Brodribb et al., 2024). Separate penetration terms were applied to production and usage emissions for countries that export vehicles to regulated markets, but do not have within country regulation (Turkey, China, South Korea, Morocco, South Africa and Mexico). Penetration rates for production emissions (e.g., charging) were applied based on the fraction of vehicles exported to regulated markets (Eurostat, 2025). China does not have regulatory incentives but imports of vehicles containing HFO-1234yf from regulated markets (e.g., Europe, USA, Japan) make up 3 %–7 % of newly registered vehicles in China (Eurostat, 2025). Based on imports

of 3 %–7 % and limited evidence of early adoption of HFO-1234yf in vehicles produced and used in China, we estimate penetration of vehicle sales to increase from 3 % in 2017 to 12 % in 2024. Penetration for domestic usage emissions (container management, operational, and end-of-life emissions), and all emissions in countries not yet mentioned, was assumed to be aligned with the HFC phasedown schedule under the Kigali Amendment to the Montreal Protocol.

2.3 Operational Emissions

Emissions that occur during the operational lifetime of the vehicle are represented by Eq. (5). This includes fugitive emissions from leaking components, sudden rupture because of component failure, and emissions during servicing.

$$E_{\text{lifetime},t,c} = \text{Bank}_{t,c} \cdot \text{EF}_{\text{OP}} \quad (5)$$

where $\text{Bank}_{t,c}$ represents the mass of refrigerant in the existing vehicle fleet in a given country and year (Eq. 6) and EF_{op} is the emission factor representing all operational emissions (%).

$$\text{Bank}_{t,c} = \sum_{t-d}^{t} (N_{\text{sales}} \cdot \text{charge} \cdot P_{\text{sales}}) \quad (6)$$

where N_{sales} is the number of vehicles sold in each country, charge is the average mass (g) of refrigerant in an individual MAC unit, and P_{sales} is the penetration of HFO-1234yf for vehicle sales in each country. Subscript d represents the vehicle lifetime for the given country.

2.4 End-of-life Emissions

The end-of-life emissions term (Eq. 7) represents emissions which occur from scrapped vehicles.

$$E_{\text{end-of-life},t,c} = M_{t-d} \cdot \eta_{\text{res}} \cdot \text{EF}_{\text{rec}} \quad (7)$$

where $M_{t-d,\text{c}}$ represents the amount of refrigerant charged into new equipment $t-d$ years prior, in the country where the vehicle was sold (see Eq. 3), η_{res} is the residual charge remaining at the point of disposal, and EF_{rec} is the percentage of this not recovered at the point of disposal. Country-level vehicle lifespan data (d) was sourced from Held et al. (2021) and Nakamoto et al. (2019), or assumed to be 15 years where data was not available. The resulting mean vehicle lifetime (±one standard deviation) is 17 (±5.3) years.

2.5 Container Emissions

The container emissions term (Eq. 8) represents refrigerant remaining in containers (known as the "heel") that is not recovered. Refrigerant stored in bulk containers (used for the first charge) is assumed to be fully recovered so emissions are zero. We assume that the heel is not recovered from refrigerant stored in cylinders (used by garages) or small cans (used by individuals) and is therefore eventually emitted.

$$E_{\text{container,t,c}} = (\text{RM}_{t,c} \cdot \text{EF}_{\text{cyl}} \cdot x) + (\text{RM}_{t,c} \cdot \text{EF}_{\text{can}} \cdot (1-x)) \quad (8)$$

where RM is the mass of refrigerant used in servicing equipment (see Eq. 9), EF_{cyl} and EF_{can} are the heel (%) of cylinders and small cans, respectively, and x is the fraction of the market using cylinders for servicing (e.g., at a garage).

$$\text{RM}_{t,c} = \sum_{t-d}^{t} \frac{M_{t,c}}{\text{MAC lifetime}} \quad (9)$$

where $M_{t,c}$ represents the amount of refrigerant charged into new equipment in the country where the vehicle was sold, and MAC lifetime is the average lifespan of a mobile air-conditioning unit.

2.6 Emission Factors

An emission factor (EF) quantifies the emission rate (% yr^{-1}) of a gas per unit of activity. Here, the emission factors (with the exception of EF_{OP}; see Table 1) were taken from IPCC (2006), with the lower value for EF_{FF} and higher recovery efficiency assigned to non-Article 5 (developed) countries and the higher EF_{FF} and lower recovery efficiency to Article 5 countries (Groups 1 and 2; developing nations) as defined by the Montreal Protocol. The operational emission factor (EF_{OP}) for HFO-1234yf is not well constrained. EF_{OP} for cars produced in the 1990s and 2000s was estimated to be 2 % yr^{-1}–10 % yr^{-1} (UNEP, 2015), but the leakage rate from MACs is known to be decreasing in newer vehicles because car manufacturers have made efforts to reduce leakage rates, incentivised by the maximum allowable leakage rates under the European Directive 2006/40/EC (European Parliament and Council, 2006). Some assessments suggest leakage rates have halved between 1990 and 2010 with the expectation of further reductions (ICF International, 2011). Furthermore, HFO-1234yf is more flammable than HFC-134a, and there is an expectation that car manufacturers will make further efforts to reduce leakage rates compared to HFC-134a systems. Based on the agreement that EF_{OP} has decreased substantially over the last two decades, and the change in refrigerant systems, we estimate that a reasonable upper limit of EF_{OP} for cars produced in 2014–2024 is 6 %. Some estimates of EF_{OP} are as low as 2.7 % by 2025 (e.g., UK National Inventory Document; UNFCCC, 2025). Here, we assume EF_{OP} to be 4 (2–6) % yr^{-1}, with 2 %–6 % being the plausible range in which EF_{OP} could fall.

Given notable uncertainty in the operational emission factor and the refrigerant charge, we modelled three emissions scenarios ("low", "middle", "high"), using operational emissions of 2 %, 4 %, and 6 %, and nominal refrigerant charges of 457, 539, and 620 g, respectively. All activity data used in the inventory (passenger car production and sales, production and sales penetration factors, and vehicle lifespan) is presented in the Supplement.

2.7 HFO-1234yf Production Emissions

Estimated annual HFO-1234yf production data were compiled by Nolan Sherry Associates (NSA) for 2025 and are

Table 2. Estimated annual production and associated emissions of HFO-1234yf in Gg yr^{-1} in 2025.

Country	Production volume	Low emission estimate	High emission estimate
USA	33–36	0.12	0.64
Japan	3–4	0.01	0.01
China	13–16	0.27	1.30
India	1–3	0.03	0.16
Global total	50–59	0.43	2.11

summarised in Table 2. Data from NSA has been used in recent scientific papers (e.g., Claxton et al., 2020; Hossaini et al., 2024) and the Technology and Economic Assessment Panel (TEAP) report to the parties of the Montreal Protocol (TEAP, 2022). Analysis by NSA uses industry data and dialogue, public reports and halocarbon production capacities. Based on the HFO-1234yf production volumes provided by NSA, it is possible to estimate fugitive emissions to air using an emission factor of 2.5 (0.9–4) % for leakages from modern plants (TEAP, 2022). The countries where HFO-1234yf production is identified to occur by NSA is consistent with independent assessments (US EPA, 2022; EIA, 2025) and indicate that Europe, a known relatively large consumer in the MAC sector, is not a producer.

3 Atmospheric Model and Methods

3.1 Model Description

We have used the Frontier Research System for Global Change version of the University of California Irvine (FRSGC/UCI) CTM which has been shown to reproduce key features of tropospheric chemistry and transport well (e.g., Hou et al., 2026; Ryan and Wild, 2021; Wild et al., 2004). Here, the model was forced using variable meteorology from the European Centre for Medium-Range Weather Forecasts (ECMWF) Integrated Forecasting System (IFS; cycle 38r1) and was run at a horizontal resolution of $2.8° \times 2.8°$ and with 57 vertical levels (surface to ~ 0.1 hPa). Time-varying anthropogenic and biogenic emissions of NO_x, CO and non-methane volatile organic compounds were prescribed from the Copernicus Atmosphere Monitoring Service (CAMS) inventories: (CAMS-GLOB-ANT v6.2; AMS-GLOB-BIO v3.1; Sindelarova et al., 2022; Soulie et al., 2024). Fire emissions were taken from the GFED5 emissions inventory (van der Werf et al., 2017). The chemistry scheme is very similar to that described by Hou et al. (2026) and the simulated airmass weighted global tropospheric OH in this version of the model (averaged over 2014–2024) of 10.8×10^5 molec. cm^{-3} is within range of the ACCMIP multi-model mean of $11.1\ (\pm 1.6) \times 10^5$ molec. cm^{-3} (Naik et al., 2013). The simulated tropospheric CH_4 lifetime with respect to OH loss is 10.2 years and thus within the observationally constrained estimate of 11.2 ($\pm$1.3) reported by Prather et al. (2012).

A tropospheric degradation scheme for HFO-1234yf was added to the model. Oxidation of HFO-1234yf initiated by the hydroxyl (OH) radical (the rate-determining step) leads to the production of trifluoroacetyl fluoride ($CF_3C(O)F$) with 100 % yield (Papadimitriou et al., 2008). Here, we prescribed single step chemistry for the oxidation of HFO-1234yf to $CF_3C(O)F$ and adopt a rate constant of 1.1×10^{-12} cm^3 molec.$^{-1}$ s^{-1} (Burkholder et al., 2020). The ozonolysis of HFO-1234yf is a minor loss pathway (~ 3 %) so was not included in the degradation scheme (Khan et al., 2026). The model does not include a chlorine atom (Cl) sink of HFO-1234yf because the global chlorine field remains uncertain (Strode et al., 2020). Once formed, $CF_3C(O)F$ can then be converted to TFA through in-cloud hydrolysis. We parameterise this process based on the cloud liquid water content and hydrolysis rate as described in Hart et al. (2026). TFA is removed from the atmosphere by wet and dry deposition or reaction with OH as described in the same study. The assumed hydrolysis rates and Henry's constants for TFA and its precursors are summarised in Supplement Tables S1 and S2.

3.2 Modelling TFA production from CFC replacements

We modelled the time-varying TFA production from HFO-1234yf emissions over the period 2014 to 2024, using the country-level bottom-up emission inventory for MACs described in Sect. 2. Within country HFO-1234yf emissions were distributed following NO_x transport sector emissions as a proxy, taken at monthly resolution from the CAMS global anthropogenic emission inventory (CAMS-GLOB-ANT) v6.2 (Soulie et al., 2024). HFO-1234yf emissions were assumed to be constant throughout the year. We also ran a sensitivity test that additionally included fugitive emissions of HFO-1234yf from its production (Table 2), represented as point source releases at production facilities identified by the US EPA (US EPA, 2022). To compare the magnitude of TFA production and deposition from HFO-1234yf to that from long-lived F-gases, we also ran the model with emissions of three HCFCs (123, 124, 133a) and six HFCs (134a, 227ea, 143a, 245fa, 365mfc, 4310-mee) for 2024 (run HFC-emis; see Sect. S1). HFC-125 was not included because the TFA yield is uncertain and assumed to be small (Sulbaek Andersen et al., 2026). Comparisons of modelled surface mixing ratios to observations are shown in Supplement Fig. S1 in the Supplement. The implementation in the model of TFA production from these source gases is described in detail and evaluated in Hart et al. (2026). The model was shown to reproduce observed TFA deposition at remote Arctic sites very well but, in agreement with other studies (e.g., Henne et al., 2025; Holland et al., 2026), it was concluded that F-gases

alone cannot explain rainwater concentrations at lower latitudes.

3.3 Source-Receptor Experiments

Using idealised emission scenarios, we quantified SR relationships which describe the mass of TFA deposited in region j from HFO-1234yf emissions in region i. Source regions were chosen to represent regions where HFO use in the MAC sector is established and emissions are growing (e.g., Europe, USA) and regions where use and emissions could substantially increase in the future, including in the under-studied southern hemisphere. Using these criteria, we selected seven regions of interest (see Fig. 1) from the source regions defined in the Hemispheric Transport of Air Pollution (HTAP2) project (Koffi Lefeivre et al., 2016), and a further four receptor regions. The source regions were North America (NAM), Europe (EUR), South Asia (SAS), East Asia (EAS), South America (SAM), Sub-Saharan Africa (SAF), and Pacific (PAN; mainly covering Australia and New Zealand). The additional "receptor" regions are the Arctic ($> 66°$ N), Antarctic ($> 68°$ S), oceans (excluding ($> 66°$ N and $> 68°$ S) and Rest of Land (ROL) which includes all land area not included in the source regions, the Antarctic or Arctic; the countries within each region are listed in Table S3.

Through a series of simulations, HFO-1234yf was emitted from each of the seven source regions in turn, with emissions from all other regions switched off. For these SR experiments, we prescribed quasi-idealised HFO-1234yf emissions that remained constant over the simulation period. To reduce the uncertainty associated with modelling small perturbations, we prescribed an emission rate of 1.9 kg person^{-1} yr^{-1} of HFO-1234yf for each source region, giving regional totals on the order of 1 Tg yr^{-1}. Regional totals were distributed between individual countries using a population weighting, and within country emissions were distributed following transport sector NO_x emissions as a proxy for leakages from MACs (see Sect. 3.2).

To assess the uncertainty in our calculated SR relationships, six sensitivity studies were also performed in which key processes affecting TFA production or deposition were perturbed individually; see Table 3. These processes include cloud uptake and hydrolysis of the TFA precursor $CF_3C(O)F$, wet and dry deposition of TFA, oxidation (OH field), and interannual variability in meteorology. The adjustments in the model relative to the BASE case are described as follows.

Species-specific deposition rates are controlled in this model through specification of the Henry's law solubility constant, species pKa, and a parameter that accounts for additional scavenging of the most soluble species in convective updrafts. Uncertainty around the Henry's law constant and pKa of TFA may impact deposition rates in the model. To investigate the minimum realistic bound for the wet deposition of TFA, we assumed the minimum Henry's law constant (232 M atm^{-1}),minimum reported pKa (0.2) of TFA and no additional convective scavenging (run BASE-LOWET). To provide an estimate of the lower bound for dry deposition of TFA, the deposition velocity was halved (run BASE-LODRY).

The rate of TFA production via hydrolysis of the $CF_3C(O)F$ precursor is also dependent on the Henry's law solubility constant, the hydrolysis rate, and the cloud liquid water content which are also uncertain. Upper and lower limits of both the Henry's law solubility constants and hydrolysis rates were applied in runs BASE-MAX and BASE-MIN (see Tables S1 and S2).

Comparisons of the chemical lifetime of CH_4 in the model (10.2 years) to observation-constrained estimates (11.2 ± 1.3 years (Prather et al., 2012)) suggests that the model overestimates the abundance of OH in common with many other global models (Stevenson et al., 2020; Yang et al., 2025). To assess the associated uncertainty in atmospheric oxidation, we include a uniform OH sink through the unimolecular decomposition of OH with air mass in the model chemistry to reduce the OH bias in run BASE-OH. This increases the chemical lifetime of CH_4 from 10.2 years to 11.3 years, which is close to the observationally constrained estimate of Prather et al. (2012).

SR simulations and sensitivities were run for the year 2017, with a preceding one-year spin-up to allow species to reach steady state. To explore how SR relationships may vary with meteorological conditions, BASE-MET was run from 2000–2017 with fixed emissions of background atmospheric species and annually varying meteorology.

3.4 Definition of metrics for SR analysis

To quantify the proportion (%) of deposition within a region that occurs from HFO-1234yf emissions from foreign regions, we define Deposition from Foreign Regions (DFFR) for region x as:

$$\mathrm{DFFR}_x = \frac{\sum_{i \neq x} D_{x \leftarrow i}}{\sum_i D_{x \leftarrow i}} \times 100 \tag{10}$$

where $D_{x \leftarrow i}$ is the TFA deposition in region x from HFO emissions in i. To evaluate the influence of a specified region on deposition in foreign regions, we calculate a Deposition to Foreign Regions (DTFR) metric for region x as:

$$\mathrm{DTFR}_x = \frac{\left(D_{\mathrm{global}} - D_x - D_{\mathrm{ocean}}\right)}{D_{\mathrm{global}}} \times 100 \tag{11}$$

where D is the annual TFA deposition globally (D_{global}), in region x (D_{x}), and in global oceans (D_{ocean}). Similar metrics have been adopted in previous studies on source apportionment such as the Response to Extra-Regional Emission Reduction metric (e.g., Nawaz et al., 2023).

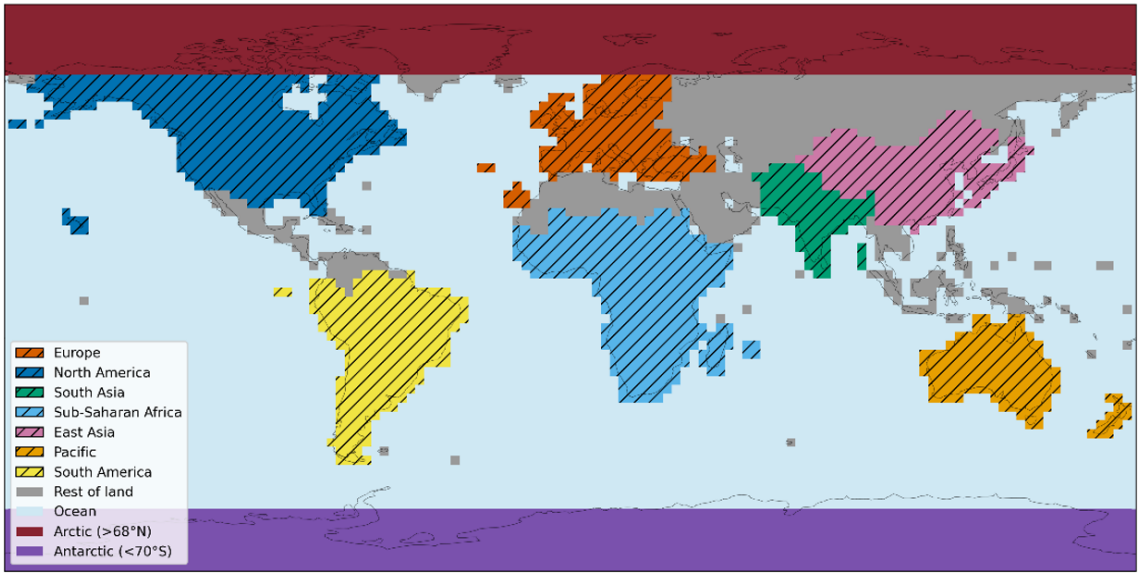


Figure 1. The eleven regions used in this study, including the seven source/receptor regions (hatched) as well as the four additional receptor regions which are Arctic (> 66° N; maroon), Antarctic (> 68° S; purple), oceans (light blue) and rest of land (grey).

Table 3. Description of each SR simulation.

Experiment	Meteorological Year	Notes and difference relative to BASE
BASE-MET	2000–2017	– Annually varying meteorology – Emissions of all other atmospheric species fixed to that of 2022 – 2017 considered as "BASE"
BASE-LODRY	2017	– Dry deposition velocity of TFA reduced by 50 %
BASE-LOWET	2017	– Minimise Henry's law constant and pKa of TFA
BASE-MIN	2017	– Set Henry's law constant to minimise TFA production and deposition – See Tables S1–S2 for the range of Henry's law constants
BASE-MAX	2017	– Maximising TFA production and deposition as above
BASE-OH	2017	Reduce model OH field bias

4 HFO-1234yf emissions and associated TFA production

4.1 Comparison of bottom-up and top-down emission estimates

Modelled global HFO-1234yf emissions from passenger vehicle MACs increased from 0.03 (0.01–0.05) Gg yr^{-1} in 2013 to 4.1 (1.8–7.0) Gg yr^{-1} in 2024. The highest emissions occur in Europe (94 % of global emissions in 2013, decreasing to 68 % in 2024), followed by North America (6 % in 2013, 15 % in 2024), and combined South Korea, Japan, and China (0 % in 2013, 16 % in 2024; see Table S4). These results reflect the timeline of regulation regarding the phase-out of HFC-134a in MACs. The European Directive 2006/40/EC on vehicle air conditioning systems banned the use of refrigerants with a GWP higher than 150 (e.g., HFC-134a) in passenger car and small commercial vehicle air-conditioning from 2017 onwards. This is notably earlier than equivalent regulations elsewhere: the phaseout in the USA occurred by 2021 under the USA SNAP directive, by 2023 under the Revised F-gas Law in Japan, and began in 2019 in Canada under the Canadian Ozone-depleting Substances and Halocarbon Alternatives Regulations (ODSHAR). Globally, most emissions in the inventory occur during operation (98 %), so the uncertainty range on our bottom-up emissions is large, reflecting the uncertainty in EF_{op}. In countries with large exports of vehicles to the European market (e.g., Mexico, Morocco, South Africa, South Korea, and Turkey), emissions associated with production are highest. End-of-life emissions are currently negligible but may substantially

increase in future because of the lag between vehicles being charged with HFO and emissions associated with their disposal. Adding production emissions to our inventory in 2024 (Table 2) increased global HFO-1234yf emissions from 4.1 (1.8–7.0) Gg yr^{-1} (MACs only) to 5.5 (2.20-9.1) Gg yr^{-1} (MACs and production).

There are currently very few published estimates of HFO-1234yf emissions with which to compare our bottom-up inventory. However, our results are in good agreement with the top-down derived emission estimates for North-West (NW) Europe (Belgium, Netherlands, Luxembourg, Germany, France, and the United Kingdom; see Fig. 2) reported by Vollmer et al (2026a). For example, our bottom-up inventory produces a NW Europe source of 1.5 (0.63–2.5) Gg yr^{-1} in the year 2023, compared to 1.5 (1.2–1.7) Gg yr^{-1} from Vollmer et al. (2026a) for the same year. Note that our emissions for the rest of Europe (EU27+EFTA+UK not including NW Europe) were 1.0 (0.45–1.8) Gg yr^{-1}in 2023. The good agreement with the top-down (observationally derived) trend supports our assumption of European uptake gradually increasing up to full substitution in 2017. Germany reports HFO-1234yf emissions of 1.2 Gg yr^{-1} in 2023 (Warncke and Gschrey, 2026) that are notably higher than both our estimate of 0.58 (0.24–0.99) Gg yr^{-1} and Vollmer et al. (2026a) of 0.42 Gg yr^{-1}in the same year. The discrepancy is explained by the higher EF_{op} used in the German inventory of 10 % yr^{-1}, compared to 4 (2–6) % yr^{-1} in our study. The assumption of EF_{OP} being 10 % yr^{-1} is considered unrealistically high for modern MAC systems (see discussion in Sect. 2.6) and this is supported by the substantial overestimation compared to top-down emissions.

A recent study estimated global emissions of HFO-1234yf to be 12 Gg yr^{-1} in 2023 (Holland et al., 2026) by scaling the top-down emissions estimate for North-West Europe of Vollmer et al. (2026a) to national GDP totals. This is notably higher than our estimate of 3.5 (1.5–6.1) Gg yr^{-1} in 2023. As discussed above, European regulation enforcing the transition away from HFC-134a occurred before the rest of the globe so emissions may not be correlated with GDP, which partially explains the discrepancy (see Fig. 3). Additionally, our inventory does not account for HFO-1234yf used in low-GWP blends (e.g., R-448A, R-449A, R-452A, R-454, R-455A and R-513A) for stationary air-conditioning. The contribution of these blends to total HFO-1234yf emissions remains uncertain but are reported by be minor ($\sim$ 5 %) in Germany (Warncke and Gschrey., 2026). Outside of Europe, estimates of HFO-1234yf emissions are scarce. However, a recent study estimated Chinese emissions of 1.5 (0.9–2.3) Gg yr^{-1} in the year 2025 (Wang et al., 2026). This estimate is based on projections that assume 100 % of the reduction in HFC emissions from MACs from the business as usual scenario to the Kigali Amendment Scenario is attributable to HFO-1234yf (Wang et al., 2023). For comparison, our bottom-up inventory produces lower Chinese HFO-1234yf emissions of 0.67 (0.41–1.8) Gg yr^{-1} from MACs and production (0.31 (0.14–0.53) Gg yr^{-1} from MACs only) in the previous year (2024).

4.1.1 Modelled HFO-1234yf mole fractions

A comparison of modelled surface mole fractions of HFO-1234yf to observations from the AGAGE global network is shown in Fig. 3. The measurements are those reported by Vollmer et al. (2026a) and include all measurements without excluding pollution events. At most sites, the model results are in reasonable agreement with the measured mole fractions, which suggests that passenger vehicle MACs are the largest source of HFO-1234yf emissions. However, an underprediction in mole fractions at Gosan (South Korea), Mace Head (Ireland), Jungfraujoch (Switzerland), Monte Cimone (Italy), and to a lesser extent Trinidad Head (USA), suggests that either a source of HFO-1234yf other than MACs could be important at these locations or that our inventory underestimates penetration or leakage rates.

Gosan (33°29′ N, 126°16′ E, 72 m a.s.l.) lies downwind of Chinese emissions and so the gap may be explained by missing HFO emissions from mainland China. Direct information on the market penetration of HFO-1234yf in Chinese vehicles is limited and may be higher than assumed here. China, along with the USA and to a lesser extent Japan and India, is a major producer of HFO-1234yf. Adding fugitive losses of HFO from production facilities (Table 2) increases the annual average modelled mole fraction at Gosan from 0.06 ppt to 0.28 ppt (upper estimate) but still underestimates the measurements of 0.41 ppt (see Fig. 3). Minor increases in modelled mole fraction are noted at all other stations. Based on the increase of 0.22 ppt per 1.3 Gg of emissions, we estimate that an additional 0.76 Gg of HFO-1234yf would need to be emitted in 2024 to explain the measurements at Gosan, giving annual emissions of 2.6 Gg $yr^{-1}$from China. This is higher than the 1.5 (0.9–2.3) Gg yr^{-1} in 2025 reported by Wang et al. (2026). The model underprediction at Mace Head is most pronounced in spring and autumn, when emissions from both North America and East Asia are most efficiently transported to Europe (Wild and Akimoto, 2001). Inclusion of production emissions from both China and the USA would decrease this discrepancy.

Direct comparison of model results with observations can be challenging given the coarse model resolution and the coastal or mountain locations of many of the measurement stations. This is particularly a problem for short-lived pollutants with strong local emissions sources where the model is unable to represent local gradients due to the assumption of numerical mixing through a grid box. This may lead to underpredictions at sites close to emission sources such as Mace Head, Jungfraujoch, and Monte Cimone (from European emissions), and Trinidad Head (from emissions in Western USA). The location of sites in coastal regions, where they may be influenced by on or off-shore flows, and in mountainous regions, where they are affected by complex terrain (Gio-

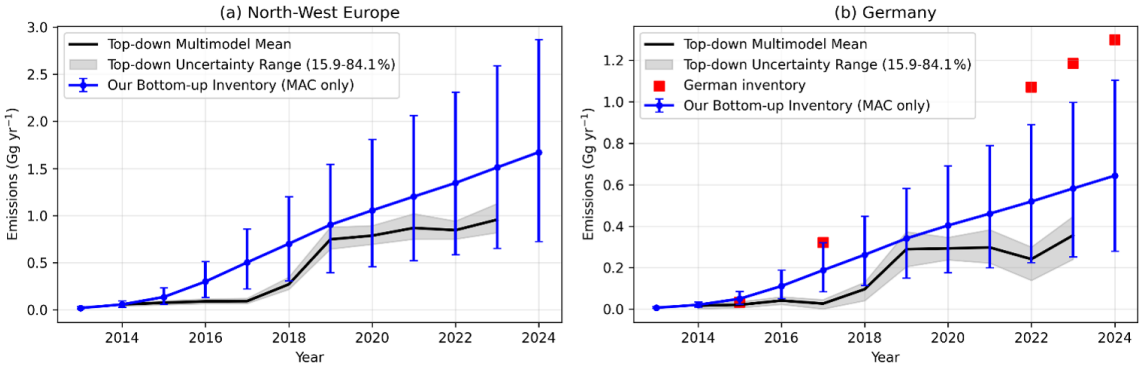


Figure 2. Bottom-up emissions of HFO-1234yf (blue; this work) in Gg yr^{-1} versus top-down emissions (black; (Vollmer et al., 2026a)) for **(a)** North-West Europe and **(b)** Germany. The error bars on the bottom-up emissions represent the low/high emissions scenarios, and the grey shading on the top-down emissions represents the uncertainty range defined by Vollmer et al. (2026a) as the 15.9 percentile of the lowest model and the 84.1 percentile of the highest model. The bottom-up emissions reported by Germany are shown in panel **(b)** in red (Warncke and Gschrey, 2026).

vannini et al., 2020) present a particular challenge. Jungfraujoch (46°55′ N, 7°99′ E, 3580 m a.s.l.) and Monte Cimone (44°12'N, 10°42'E, 2165 m a.s.l.) are mountain sites that receive both clean air masses (representing baseline concentrations) and polluted air from continental Europe (Giostra et al., 2011). While we underestimate the mole fraction when comparing to measurements including both polluted and baseline measurements (Figs. 3, S2), we find that the model results are in better agreement with measurements when those labelled as pollution events are filtered out (Fig. S3; note that agreement is also better at Gosan). This suggests these sites may be influenced by a missing source of HFO-1234yf transported in polluted airmasses from continental Europe. Henne et al. (2025) report better agreement at Jungfraujoch despite using similar emissions for Europe that may reflect better representation of mountainous terrain in a higher resolution model.

We ran an additional sensitivity test (Sensitivity 2; Fig. S4) using the 12 Gg yr^{-1} emission and spatial distribution described in Holland et al. (2026). These elevated emissions did not significantly alter the modelled European mole fractions (ZEP, MHD, TAC, TOB, JFJ, and CMN) but considerably increased the mole fraction above observed amounts at sites in the rest of the globe (notably THD, RPB and CGO), supporting our hypothesis that the transition to HFOs in Europe has occurred ahead of the rest of the globe. Note that the modelled mole fractions reported by Holland et al. (2026) are in good agreement with observations outside of Europe (e.g., CGO, RPB, and THD) whereas our modelled mole fractions are substantially higher than these observations with the same emissions (see Fig. S4). This can be explained by faster removal of HFO-1234yf by OH (12 d) in their model than ours (14 d in Sensitivity 2), resulting in a lower atmospheric burden from the same emissions. Typical of a short-lived species, the global lifetime of HFO-1234yf depends on the relative size of emissions in different regions so comparing the lifetime of a well-mixed species is a better indicator of the OH field. For example, the lifetime for Sensitivity 1 (including production emissions) is 16 d, increasing to 18 d averaged over the simulations from 2014-2024. Holland et al. (2026) report an atmospheric lifetime of nine years for HFC-134a, whereas the longer lifetime with respect to tropospheric oxidation of 13 years in our model is in better agreement with the observationally constrained lifetime of 15.7 ± 1.9 years reported by (Prather et al., 2012).

4.1.2 Modelled TFA deposition from HFO-1234yf, HCFCs, and HFCs

Global TFA deposition from HFO-1234yf use in the MAC sector increased from 0.078 (0.050–0.17) Gg yr^{-1} in 2014 to 3.5 (1.6–6.4). The inclusion of fugitive HFO-1234yf emissions during its production increases the 2024 estimate to 5.1 (1.8–8.5) Gg yr^{-1}. TFA deposition from HCFCs (123, 124, 133a) and HFCs (134a, 143a, 227ea, 365mfc, 245fa, 43-10mee) was 22 Gg yr^{-1} in 2024. We thus estimate that HFO-1234yf accounted for up to 28 % of global total TFA deposition from CFC replacements in 2024. Production emissions are included in this estimate because the contribution from HCFC/HFCs implicitly includes fugitive emissions from production. While HCFCs and HFCs are now being phased out/down under various amendments to the Montreal Protocol, they remain an important atmospheric TFA source because of the large banks and the long atmospheric lifetimes of HCFCs/HFCs (Hart et al., 2026). Additionally, their emissions are presently substantially higher than HFO-1234yf (see Table S5) and this work shows that at present they remain the dominant atmospheric TFA source on a global basis. Similarly, Holland et al. (2026) estimate that TFA deposition from HFO-1234yf is equivalent to 26 %–75 % of global deposition attributable to HFC-134a. Holland et al. (2026) prescribe considerably higher annual HFO-1234yf emissions

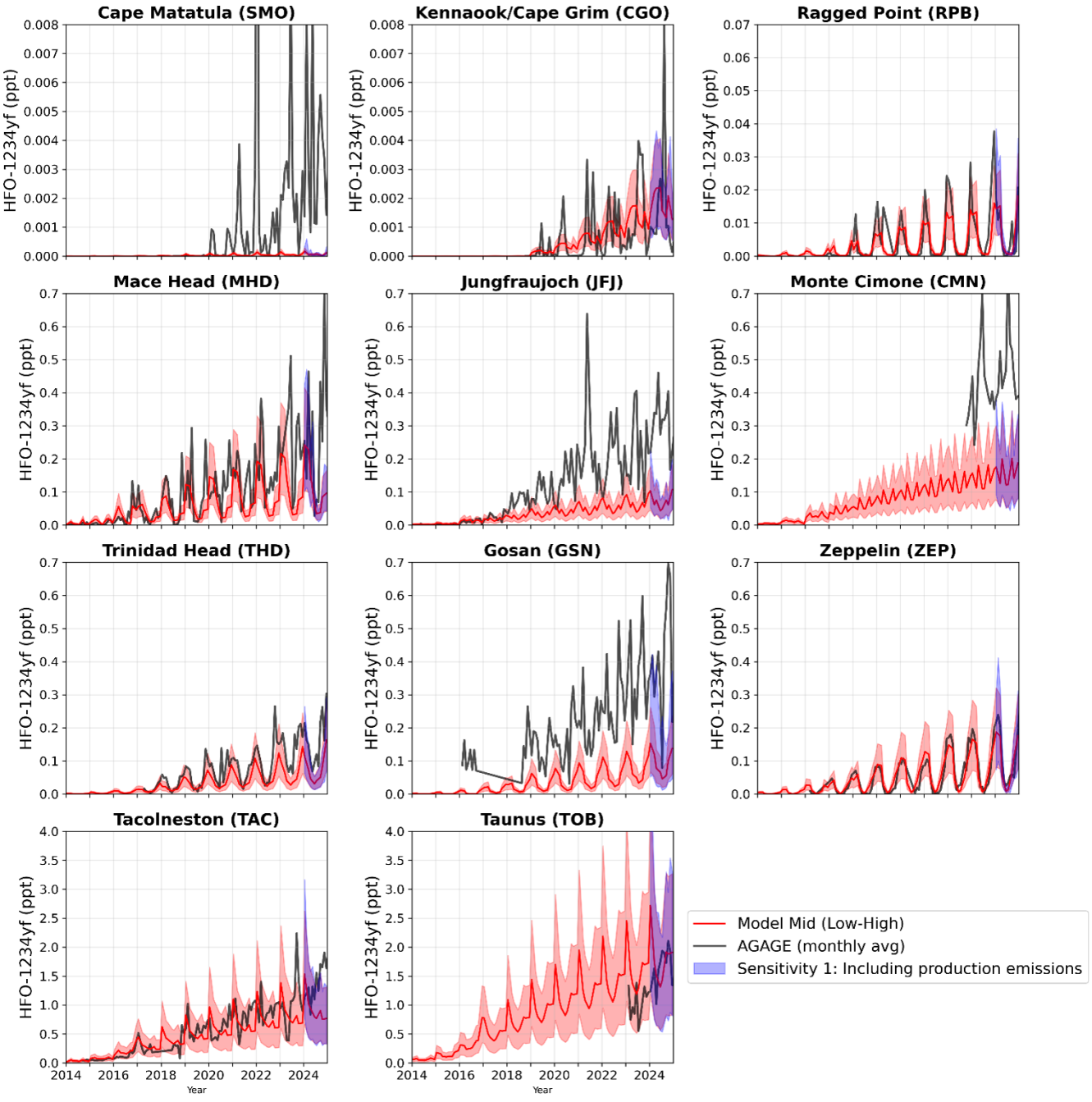


Figure 3. Modelled monthly mean surface mole fractions of HFO-1234yf in ppt from the middle emissions scenario (red line), low and high bounds (red shading), and observed mole fractions (black) at AGAGE measurement stations (Vollmer et al., 2026a). Monthly mean mole fraction from a sensitivity run with additional production emissions in 2024 are shown in blue.

of 12 Gg yr^{-1} in 2023 compared to 3.5 Gg yr^{-1} in our model and thus predict a higher production of TFA of 11.1 Gg yr^{-1}.

At the regional scale HFO-1234yf (including emissions from MACs and production) contributes up to 56 % of TFA deposition from CFC replacements in Europe, 43 % in North America, and 39 % in East Asia in 2024, showing that it is an important emerging source in some regions. In the OH corrected sensitivity runs the proportions are slightly lower at 52 % in Europe, 36 % in North America, and 30 % in East Asia. Henne et al. (2025) predict a higher TFA deposition rate from HFO-1234yf than our model (see Fig. S5) and thus report a higher contribution of 2.4–5 times that of the long-lived CFC replacements in Europe. Regional differences in HFO-1234yf contribution are a result of the notable

differences between the spatial distribution of TFA produced from long-lived CFC replacements (HCFCs and HFCs), and HFO-1234yf (Fig. 4). TFA deposition from HFO-1234yf is largely confined to the Northern hemisphere, with the highest deposition rates in Europe, the Atlantic, and East Asia rather than in the tropics and midlatitudes for its source from HCFCs and HFCs. The highest deposition rate from HFO-1234yf (90 $\mu g\,m^{-2}\,yr^{-1}$) occurs in Europe (Fig. 4a), whereas the highest TFA deposition from HCFCs/HFCs occurs in China (173 $\mu g\,m^{-2}\,yr^{-1}$; Fig. 4b). Uptake of HFO-1234yf in MACs in China is projected to increase so China may become a deposition hotspot of TFA from HFO-1234yf in the future.

5 Source-receptor relationships

HFO-1234yf is an emerging TFA source and its emissions are increasing in both distribution and magnitude as countries transition from HFCs to HFOs. Therefore, it is valuable to look at SR relationships to understand the implications of future emissions from regions that are currently low emitters of HFO-1234yf. This section uses idealised emission scenarios to explore these SR relationships.

The relationship between HFO-1234yf emissions in region i and TFA deposition in region j is quantified by a SR influence function I_{ij}, defined by Corbitt et al. (2011) as:

$$I_{ij} = D_{ij}/E_i \quad (12)$$

where D_{ij} is the total deposition to receptor region j from emissions E_i in region i. Figure 5 shows the influence functions I_{ij} for each of the SR region pairs and the corresponding TFA deposition footprints for each emissions region are shown in Fig. 6.

Generally, TFA deposition occurs within the same hemisphere as HFO-1234yf emissions, but extra-regional deposition dominates (87 %–96 %). In the Northern Hemisphere, prevailing westerly winds transport pollution from North America to Europe, Europe to Russia and the Middle East, and East Asia towards North America. These transport patterns are well documented (e.g., Jacob et al., 1999; Wild and Akimoto, 2001), and the effects of this can be seen in the EAS-NAM, EUR-NAM, and EUR-ROL (note that 60 % of deposition in ROL from European emissions occurs in Russia) SR pairs (Fig. 5). Nonetheless, a larger proportion of European TFA is deposited in NAM than vice versa via either transatlantic easterly flows, or westerlies around the globe (Wild and Akimoto, 2001). This is also influenced by the longer lifetime of HFO-1234yf emitted in EUR (calculated to be 18 d) than NAM (16 d; see Table S6), allowing transport further from the emission region. The relatively coarse resolution used in our model ($2.8° \times 2.8°$) introduces uncertainty in calculating within-region and extra-regional deposition fluxes. Numerical mixing within large grid boxes can dilute near source concentrations, and transport is more diffusive, so the low-resolution may cause a negative bias in calculated within-region deposition fractions.

Consistent with other modelling studies, we find that most TFA is deposited outside of the HFO emission regions (e.g., David et al., 2021; Henne et al., 2012; Khan et al., 2026; Wang et al., 2024). Our summer within-region deposition fraction of 13 % in North America is in reasonable agreement with the 17 % reported by Kazil et al. (2014) from a 2.5-month simulation over summer but considerably lower than Khan et al. (2026), Henne et al. (2012), and Wang et al. (2024) who estimate domestic fractions for Europe, North America and Asia ranging from 30 %–42 %. The SR relationships here are sensitive to differing Henry's law constants and wet and dry deposition parameterisations (see Fig. S6) so model parameterisation may explain differences in results. Some studies (e.g., Henne et al., 2012) use the Henry's law constant of nitric acid which is higher than that of TFA and assume instant hydrolysis of TFA precursors when cloud water is present in a grid cell. A Henry's law limited partitioning of the precursor, as we include in this model, could result in more widespread TFA deposition (Kazil et al., 2014). The inter-model differences in deposition schemes are highlighted by the variety of wet to dry deposition ratios reported between studies. The only reported observed mean wet deposition proportion is 55 % in Toronto (Persaud et al., 2026). In Europe we estimate 64 %, but Henne et al. (2025) and Holland et al. (2026) report a much higher wet deposition proportion of 94 % and 88 %–92 %, respectively and this will alter the spatial distribution of TFA deposition. Further, differences in OH fields between models and the inclusion of the highly uncertain Cl oxidation in some models may explain some of the differences. Given the substantial model differences, an inter-model comparison project would be valuable. Although there is considerable variation between model estimates of within-region deposition fractions, the qualitative agreement across models indicates that widespread deposition of TFA away from HFO-1234yf sources is robust.

This is the first study to model HFO-1234yf emissions from regions in the southern hemisphere, which have not been considered in previous studies. We find that trade winds from Sub-Saharan Africa transport TFA to South ($I_{ij} = 8\,\%$) and Central America and TFA from South American emissions is transported across (and deposited in) the southern Atlantic on westerlies with some TFA deposited in Sub-Saharan Africa ($I_{ij} = 4\,\%$). A notable finding of our analysis is that a large amount of TFA produced by HFO-1234yf is deposited to the ocean rather than to land. Ocean deposition ranges from 43 %–75 % depending on the HFO-1234yf source region (Fig. 5), with the average of 54 % consistent with the 55 % reported by Khan et al. (2026). A particularly high proportion of TFA is deposited to the oceans from emissions in PAN (75 %) and SAM (66 %), because of the small land area in proximity. The impacts of this deposition on the marine environment are not well known because the toxicity of TFA has only been studied on two marine species to date (Han-

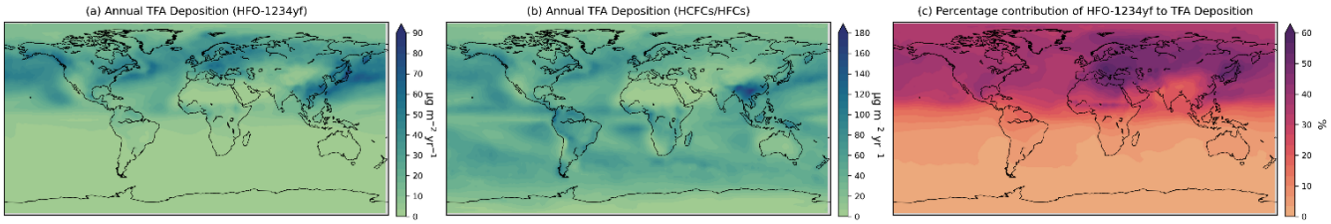


Figure 4. Modelled annual TFA deposition ($\mu g\,m^{-2}\,yr^{-1}$) for the year 2024 from **(a)** HFO-1234yf MAC and production emissions (upper estimate) and **(b)** HCFC and HFC emissions, and **(c)** the percentage of TFA deposition from CFC replacements attributable to HFO-1234yf. The deposition quantity is the sum of wet and dry deposition.

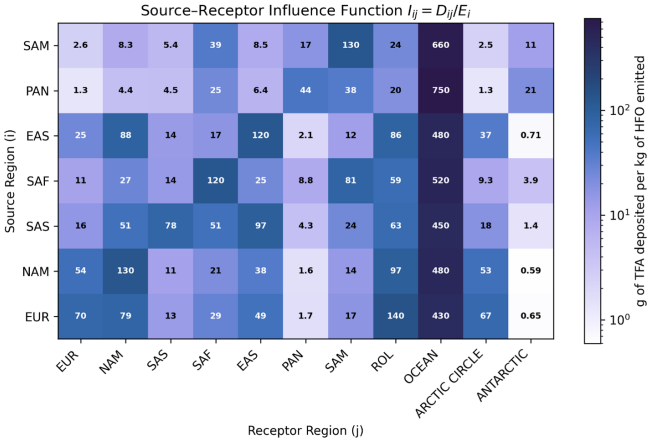


Figure 5. Source receptor influence matrix presenting the mass (g) of TFA deposited in region j from HFO-1234yf emissions (kg) in region i. EUR = Europe, NAM = North America, SAS = South Asia, SAF = Sub-Saharan Africa, EAS = East Asia, PAN = Pacific, SAM = South America, ROL = rest of land. Note that ROL, OCEAN, ARCTIC CIRCLE, and ANTARCTIC are receptor regions but not considered as sources in this study.

son et al., 2024). Elevated land deposition fractions in other regions will increase TFA accumulation in freshwater, soil, plants, groundwater and crops and increase exposure of humans and animals.

From ice core records, studies have shown increasing deposition of TFA in the Arctic (Hartz et al., 2023; Pickard et al., 2020) and Antarctica (Li et al., 2026). Our recent work (Hart et al., 2026) has shown that long-lived precursors (HCFCs and HFCs) can explain historical observed Arctic TFA deposition trends. The SR relationships quantified here can inform us on the regions contributing to TFA measured in polar regions which can act as a sink for persistent pollutants (Raheem et al., 2025). The TFA deposition efficiency in the Arctic is highest for HFO-1234yf emissions from EUR, NAM, and EAS, with $I_{ij} = 7\,\%$, $5\,\%$, and $4\,\%$, respectively. This is consistent with a HTAP study which found that EUR, NAM and EAS were all important source regions for short-lived pollutants such as ozone, aerosols, and CO to the Arctic (Shindell et al., 2008). Historically, the ice core record represented global TFA deposition because it was mainly produced from long-lived compounds and European HFO-1234yf emissions that can be transported to the Arctic. However, as HFO-1234yf emissions are expected to grow in regions with a lower influence on the Arctic, such as South and East Asia (Wang et al., 2026), the Arctic deposition record may no longer reflect trends in global TFA deposition. This highlights the need for increased rainwater monitoring at lower latitudes to show the true increase in TFA deposition as a result of the transition to HFOs. Deposition from PAN and SAM reaches Antarctica ($I_{ij} = 2\,\%$ and $1\,\%$, respectively), and the Southern Ocean (Fig. 6). TFA deposition fluxes inferred from Antarctic ice cores have been increasing since 1990 (Li et al., 2026), before the use of HFOs, but our results indicate that source regions exert a limited influence on Antarctica. This observed TFA is likely derived from precursors other than HFO-1234yf, such as the long-lived CFC replacements (HCFCs/HFCs).

5.1 Regional vulnerability to TFA deposition

While future emissions of HFOs remain uncertain, the SR relationships can inform us on the potential vulnerability of a region to future TFA deposition. Vulnerability is influenced by the proportion of deposition that occurs from foreign regions (DFFR metric; Eq. 10), and the proportion of domestic TFA deposition (see Fig. 5), which is affected by the regional lifetime of both HFO-1234yf and atmospheric TFA. The results (shown in Table 4) are calculated from idealised emission scenarios and are therefore indicative rather than absolute because the relative contribution of different regions will depend on their actual emissions.

The proportion of regional deposition from foreign emissions is highest in North America ($85\,\%$), Sub-Saharan Africa ($89\,\%$), and Pacific ($90\,\%$), and this can be explained by their SR relationships. North America receives substantial deposition from Europe and East Asia, while Sub-Saharan Africa receives contributions from all source regions. These three regions may receive disproportionate TFA deposition relative to their own emissions, and global scale policies would be required to reduce TFA pollution here. In contrast, South Asia receives a relatively low proportion of deposi-

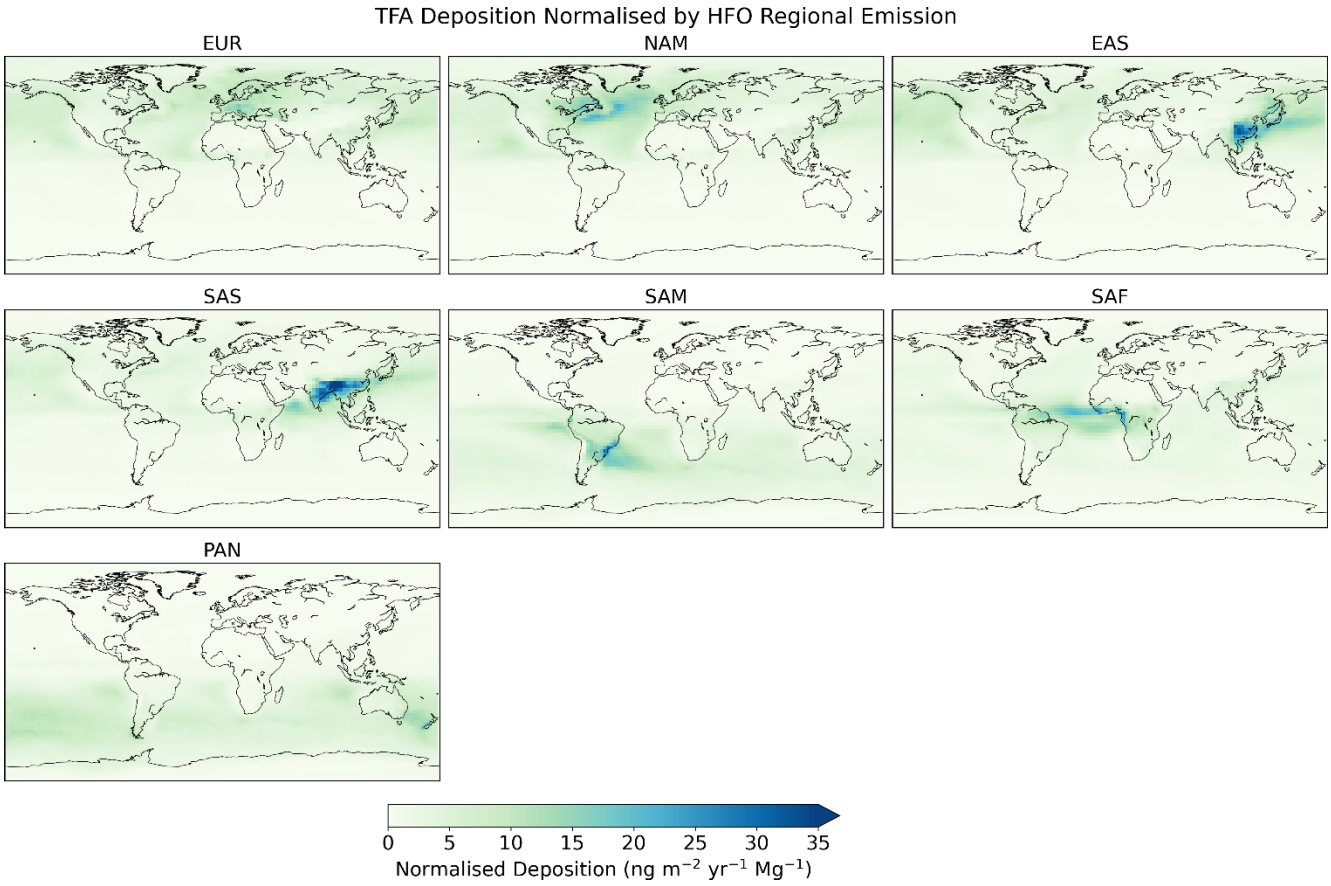


Figure 6. The deposition footprint (ng m^{-2} yr^{-1}) of TFA per Mg of HFO-1234yf emitted in each source region, normalised by the regional emission. The dark blue areas are places of high TFA deposition as a result of HFO-1234yf emissions in the given source region.

Table 4. Percentage of TFA deposition within a region that occurs from HFO-1234yf emissions from foreign regions (DFFR) and the percentage of TFA deposition that occurs in foreign regions from HFO-1234yf emissions in a specified region (DTFR).

Region	DFFR (%)	DTFR (%)
South Asia	19	38
East Asia	54	31
North America	85	32
Europe	65	43
Pacific	90	13
South America	65	13
Sub-Saharan Africa	89	27

tion from foreign emissions so regional emissions reductions would be more effective here.

A low proportion of emissions from Sub-Saharan Africa, Pacific, and South America are deposited in foreign regions (DTFR metric) owing to limited land in proximity, but Sub-Saharan Africa and Pacific receive high levels of deposition from foreign emissions. Conversely, over a third of deposition from Europe and South Asia occurs in foreign land regions, reflecting their continental positions, and emissions reductions in these regions would be impactful for their receptor regions. These results highlight the vulnerability of North America, Pacific, and Sub-Saharan Africa to high TFA deposition rates from global HFO-1234yf emissions. They also demonstrate that emissions reductions in the northern hemisphere (Europe, South Asia, East Asia, and North America) would provide the greatest benefits in reducing transboundary TFA deposition.

5.2 Source-receptor relationships based on bottom-up emissions

Here, we scale the source-receptor influence functions calculated from the idealised emissions to our own bottom-up emission inventory from MACs to examine the impacts of historical HFO-1234yf emissions on receptor regions. We quantify cumulative TFA deposition over the period 2013–2024 in each region attributable to foreign HFO-1234yf emissions from the bottom-up inventory using the imports metric (Table 5). The imports metric is defined as the TFA deposited within a given region attributable to HFO-1234yf

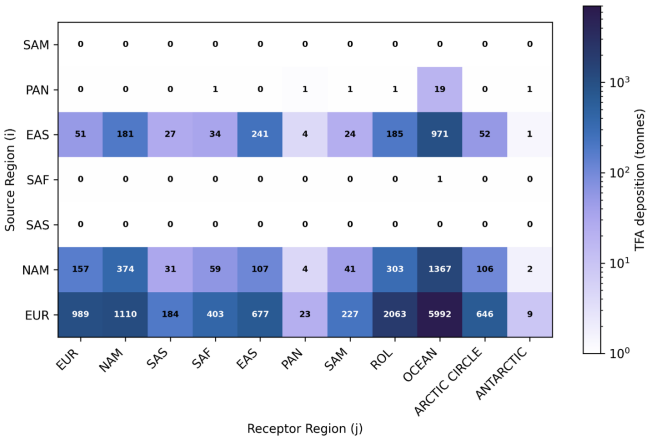


Figure 7. Matrix presenting TFA deposition (t) in each receptor region j from bottom-up HFO-1234yf emissions in source region i, calculated as the product of I_{ij} and E_i where E_i is the cumulative emission total of countries in region i over the years 2013–2024.

emissions from other regions, and exports is the TFA deposited in foreign land regions attributable to HFO-1234yf emissions from that region (note that this excludes ocean and the poles). EUR is the only region where exports exceed imports, highlighting its importance as a net atmospheric 'exporter' of TFA deposition outside of its borders. It has the largest emissions of all regions, and TFA produced from European emissions reaches all receptor regions, although influence on regions in the Southern Hemisphere is minor (see Fig. 7). NAM and EAS are the next largest emitters of HFO-1234yf; however, both receive more than twice the amount of atmospheric TFA that they export. In both cases, EUR is the primary source of imported TFA. Although at present, significant HFO-1234yf emissions are confined to EUR, NAM, and EAS, all receptor regions receive some TFA deposition through long-range transport. Over the study period, we estimate that the global ocean has received the greatest amount of TFA (8350 t), followed by ROL (2551 t), and NAM (1665 t). Note that production emissions were not included in this analysis because data was only for a single year and their addition would increase the atmospheric exports from NAM and EAS.

5.3 Uncertainties in SR relationships

We identified the key uncertainties in the model representation of TFA production and deposition and explored the sensitivity of the model results to these through a series of sensitivity tests. These tests include modifying the treatment of wet and dry deposition (BASE-LOWET/LODRY), Henry's law solubility constants (BASE-MIN/MAX), and the OH abundance controlling HFO oxidation (BASE-OH). In each simulation, a single uncertain parameter or process was perturbed relative to the BASE configuration, while all other settings were held constant (see Table 3). Figure 8 shows the

Table 5. Cumulative TFA imports (t) and exports (t) over the period 2013–2024.

Region	Imports (t)	Exports (t)
EUR	210	2600
NAM	1300	400
SAS	240	0.0
SAF	500	0.20
EAS	790	320
PAN	32	2.0
SAM	290	0.0
ROL	2600	100

deviation from the BASE results for each sensitivity test. Additional uncertainty arises from omitting the Cl sink of HFO-1234yf in the model. This was not evaluated because assessments have found that there are wide variations in the global chlorine distribution and magnitude between models, and it remains unclear which Cl fields are best (Strode et al., 2020). Previous work suggests Cl may account for 16 % (Henne et al., 2012) but based on the most recent estimates of [Cl], the sink is expected to be relatively minor (∼ 4 %), despite a faster rate constant.

TFA deposition was most sensitive to uncertainties in the Henry's law constant and hydrolysis rate (runs BASE-MAX and BASE-MIN). The solubilities of TFA and its precursor $CF_3C(O)F$ are highly uncertain, and modelled TFA deposition rates have been shown to be sensitive to the Henry's law constant used (Hart et al., 2026; Killen et al., 2026). BASE-MAX decreased the proportion of deposition occurring in foreign regions (DTFR) by 3 %–14 % and reduced the ocean fraction by 1 %–12 %, with corresponding increases of 2 %–6 % (DTFR) and 0 %–8 % (ocean fraction) in BASE-MIN. These results can be explained by faster hydrolysis of the precursor and increased wet deposition rates in BASE-MAX, resulting in TFA being deposited closer to emissions regions, and the converse in BASE-MIN. The calculated I_{ij} metrics are also sensitive to this uncertainty (see Fig. S6), with increases of up to 100 % (SAF) for domestic deposition in BASE-MAX/MIN.

Uncertainty in the solubility of TFA also contributes to uncertainties in wet and dry deposition rates and their relative importance (see BASE-LOWET), as does uncertainty in the pKa of TFA, and the dry deposition velocity used in the model (see BASE-LODRY). The magnitude of TFA deposition is not sensitive to differences in deposition schemes (< 5 % in BASE-LOWET and BASE-LODRY; Fig. 8a) because of compensation between the two pathways (Fig. 8c). However, decreasing wet deposition results in more widespread TFA deposition, and ocean fraction and DTFR reduce correspondingly (Fig. 8b, d). Uncertainty in the relative importance of wet and dry deposition should be noted when comparing model results to observed rainfall concen-

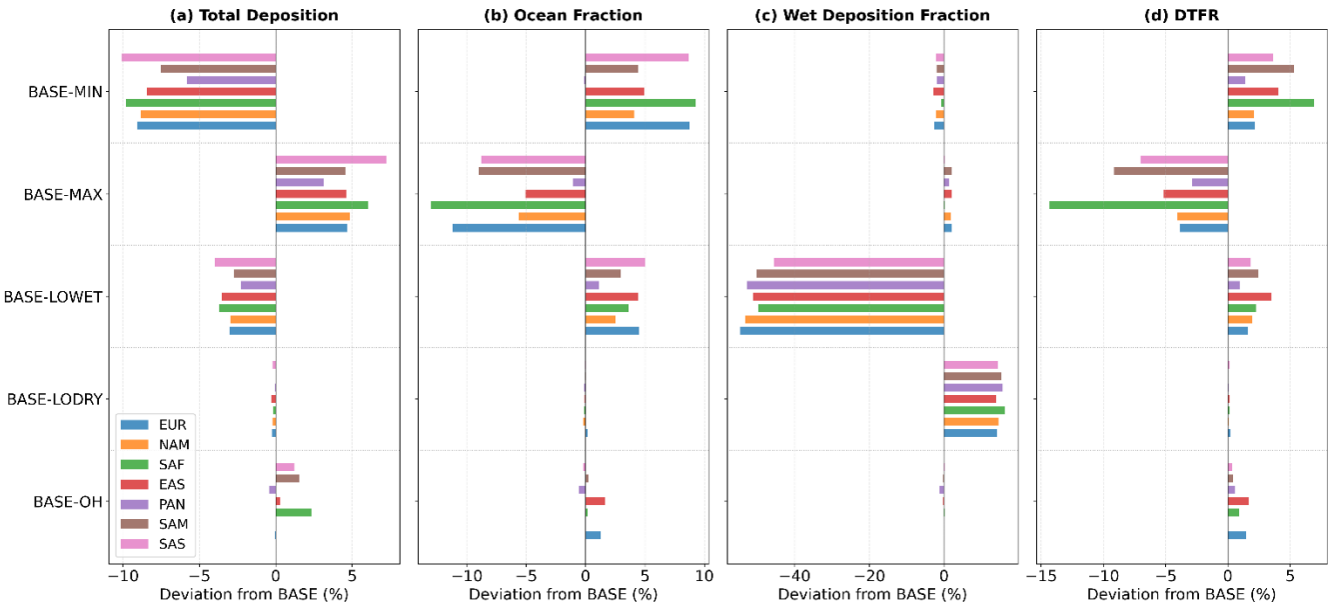


Figure 8. Percentage deviations from the BASE run for each region in each sensitivity test for metrics **(a)** Total deposition, **(b)** ocean fraction, **(c)** wet deposition fraction, and **(d)** DTFR.

trations. Here, wet deposition accounts for 66 % of total deposition in run BASE, which compares well with the only available measurements of wet and dry deposition independently with a median of 63 % wet deposition (Persaud et al., 2026).

We also explored the sensitivity of the SR relationships to potential biases in OH, and thus oxidation capacity, in the model (run BASE-OH). Calibrating model OH to the observed methane lifetime reported by Prather et al. (2012) reduced the global annual burden of OH by 27 % (see Fig. S7), increasing the global lifetime of HFO-1234yf from 18 to 22 d. However, the impact of the OH bias on SR relationships was comparatively low compared to other sensitivity tests (see Fig. 8), with deviations of < 3 % on the ocean fraction and DTFR, and minor impacts on I_{ij} values (see Fig. S6).

To examine the differences in TFA deposition due to interannual variability in meteorology, we ran a simulation (BASE-MET) over 18 years, with a fixed background atmospheric composition (i.e. background trace gas concentrations) to isolate the meteorological effects. The interannual differences in TFA deposition to each receptor region are shown in Fig. S8. Consistent with the results of David et al. (2021), interannual variability in deposition is small (the mean coefficient of variation across receptor regions is 7 %), confirming that it is appropriate to apply source-receptor relationship calculated for a given year (e.g., 2017) to any other year.

6 Summary and Conclusions

We present a global bottom-up emissions inventory of HFO-1234yf from passenger vehicle mobile air conditioning systems (MACs). The inventory considers emissions from vehicle first fill, servicing, operation and end-of-life disposal, with country-wise assumptions around HFO market penetration in the MAC sector. We estimate that global emissions increased rapidly from 0.03 (0.01–0.05) Gg yr^{-1} in 2013 to 4.1 (1.8–7.0) Gg yr^{-1} in 2024 with the largest contributions from Europe (68 % in 2024), but with substantial contributions from North America (15 %) and East Asia (16 %). For NW Europe, our bottom-up emissions agree well in both trend and magnitude with a recent top-down estimate. Inclusion of these emissions in the FRSGC/UCI CTM results in reasonably good agreement between the model and surface HFO-1234yf observations from the AGAGE network. China and the USA (and to a lesser extent Japan and India) are major producers of HFO-1234yf and including an estimate of fugitive emissions during its production increased global emissions to 5.5 (2.2–9.1) Gg yr^{-1} in 2024. While inclusion of production emissions improved agreement with measurements, the model still underestimated the observed mole fractions in East Asia. This is attributed in part to uncertainty in the take up of HFO-1234yf in domestically used MAC systems in this region.

We have shown that global TFA deposition from HFO-1234yf in MACs has increased from 0.078 (0.050–0.17) Gg yr^{-1} in 2014 to 3.5 (1.6–6.4). Despite this increase, TFA production from HFO-1234yf (including emissions from MACs and production) only made up 28 % of

global total production from all CFC replacements (HCFCs, HFCs, and HFO-1234yf) in 2024. HFO-1234yf is an important emerging source in Europe, North America, and East Asia where it contributes to 56 %, 43 %, and 39 % of TFA deposition from CFC replacements, respectively. This balance is likely to change in future as regulation-driven substitution of HFCs increases and the transition is shifting TFA deposition from the tropics towards northern Europe and mid-latitudes. While deposition from HFO-1234yf emissions is more closely aligned with the region of emission, quantification of SR relationships shows that transboundary deposition remains dominant, with the majority of TFA deposited over the oceans. Source regions in the southern hemisphere have the highest oceanic deposition fractions and least impact on other terrestrial regions.

Our findings raise environmental justice concerns. European HFO-1234yf emissions account for the majority of global cumulative TFA deposition due to HFO-1234yf, while all other regions atmospherically import more than twice the amount of TFA than they export. These findings underscore the need for global policy to reduce TFA deposition from HFO-1234yf while understanding of the toxicity and environmental effects of TFA is still evolving (e.g., Cousins et al., 2019). Constraint of key uncertainties would strengthen these findings – particularly the Henry's law solubility constants of TFA and its precursors, and quantification of HFO-1234yf emissions beyond MACs, including production and stationary air conditioning emissions.

Data availability. Activity data including car sales and production, penetration factors, and vehicle lifetime are detailed in Supporting Information. Our bottom-up emission inventory is available in Supporting Information. Model outputs containing the time series of TFA deposition from HFO-1234yf, and HFO-1234yf emissions and TFA deposition from each region of the source receptor experiments are available at https://doi.org/10.5281/zenodo.21458539 (Hart, 2026). AGAGE observations are available at https://doi.org/10.5281/zenodo.20020038 (Vollmer et al., 2026b).

Supplement. The supplement related to this article is available online at https://doi.org/10.5194/acp-26-16683-2026-supplement.

Author contributions. LH, RH, OW: conceptualisation; LH: atmospheric chemistry simulations and analysis; MV: expertise on atmospheric networks and observations; DS: production emission estimates; RH, OW, CH: supervision; LH: writing of original draft; all authors: writing, review, and editing.

Competing interests. The contact author has declared that none of the authors has any competing interests.

Disclaimer. Publisher's note: Copernicus Publications remains neutral with regard to jurisdictional claims made in the text, published maps, institutional affiliations, or any other geographical representation in this paper. The authors bear the ultimate responsibility for providing appropriate place names. Views expressed in the text are those of the authors and do not necessarily reflect the views of the publisher.

Acknowledgements. We thank Ray Gluckman for his advice on HFO-1234yf emissions.

Financial support. This research has been supported by the Natural Environment Research Council (grant nos. NE/V013041/1, NE/V011863/1, and NE/X003582/1).

Review statement. This paper was edited by Ivan Kourtchev and reviewed by two anonymous referees.

References

ACEA (European Automobile Manufacturers' Association): New cars in the EU by segment, https://www.acea.auto/figure/new-passenger-cars-by-segment-in-eu/, last access: 31 June 2025.

Arp, H. P. H., Gredelj, A., Glüge, J., Scheringer, M., and Cousins, I. T.: The global threat from the irreversible accumulation of trifluoroacetic acid (TFA), Environ. Sci. Technol., 58, 19925–19935, https://doi.org/10.1021/acs.est.4c06189, 2024.

Brodribb, P., McCann, M., Dewerson, G., Franjić, J., and Anderson, G.: Cold Hard Facts 4, report prepared for the Department of Climate Change, Energy, the Environment and Water, Canberra, Australia, https://www.dcceew.gov.au/environment/protection/ozone/publications/cold-hard-facts-4 (last access: 9 November 2026), 2024.

Burkholder, J. B., Sander, S. P., Abbatt, J., Barker, J. R., Cappa, C., Crounse, J. D., Dibble, T. S., Huie, R. E., Kolb, C. E., Kurylo, M. J., Orkin, V. L., Percival, C. J., Wilmouth, D. M., and Wine, P. H.: Chemical Kinetics and Photochemical Data for Use in Atmospheric Studies, Evaluation No. 19, JPL Publication 19-5, Jet Propulsion Laboratory, Pasadena, https://dataverse.jpl.nasa.gov/dataset.xhtml?persistentId=hdl:2014/49199&version=2.1, last access: 1 May 2020.

Claxton, T., Hossaini, R., Wilson, C., Montzka, S. A., Chipperfield, M. P., Wild, O., Bednarz, E. M., Carpenter, L. J., Andrews, S. J., Hackenberg, S. C., Mühle, J., Oram, D., Park, S., Park, M.-K., Atlas, E., Navarro, M., Schauffler, S., Sherry, D., Vollmer, M., Schuck, T., Engel, A., Krummel, P. B., Maione, M., Arduini, J., Saito, T., Yokouchi, Y., O'Doherty, S., Young, D., and Lunder, C.: A synthesis inversion to constrain global emissions of two very short lived chlorocarbons: dichloromethane and perchloroethylene, J. Geophys. Res.-Atmos., 125, e2019JD031818, https://doi.org/10.1029/2019JD031818, 2020.

Corbitt, E. S., Jacob, D. J., Holmes, C. D., Streets, D. G., and Sunderland, E. M.: Global source–receptor relationships

for mercury deposition under present-day and 2050 emissions scenarios, Environ. Sci. Technol., 45, 10477–10484, https://doi.org/10.1021/es202496y, 2011.

Cousins, I. T., Ng, C. A., Wang, Z., and Scheringer, M.: Why is high persistence alone a major cause of concern?, Environ. Sci.-Processes Impacts, 21, 781–792, https://doi.org/10.1039/c8em00515j, 2019.

Database26: Complete refrigerant capacity chart (R134a, R1234yf), along with A/C compressor oil filling quantities, https://database26.com/refrigerant-capacity-chart-r134a-r1234yf/, last access: 18 December 2025.

David, L. M., Barth, M., Höglund-Isaksson, L., Purohit, P., Velders, G. J. M., Glaser, S., and Ravishankara, A. R.: Trifluoroacetic acid deposition from emissions of HFO-1234yf in India, China, and the Middle East, Atmos. Chem. Phys., 21, 14833–14849, https://doi.org/10.5194/acp-21-14833-2021, 2021.

Environmental Investigation Agency (EIA): Persistent Problems: The hidden impacts of hydrofluoroolefins, the latest generation of fluorinated gases, EIA UK, London, UK, https://eia-international.org/report/persistent-problems/ (last access: 28 October 2026), 2025.

European Chemicals Agency (ECHA): Registry of CLH intentions until outcome – trifluoroacetic acid, ECHA, Helsinki, Finland, https://echa.europa.eu/registry-of-clh-intentions-until-outcome/-/dislist/details/0b0236e188e6e587 (last access: 30 July 2026), 2026.

European Parliament and Council: Directive 2006/40/EC of the European Parliament and of the Council of 17 May 2006 relating to emissions from air conditioning systems in motor vehicles and amending Council Directive 70/156/EEC (Text with EEA relevance), Document 32006L0040, MAC directive EU, https://eur-lex.europa.eu/eli/dir/2006/40/oj (last access: 19 November 2026), 2006.

Ellis, D. A., Mabury, S. A., Martin, J. W., and Muir, D. C. G.: Thermolysis of fluoropolymers as a potential source of halogenated organic acids in the environment, Nature, 412, 321–324, https://doi.org/10.1038/35085548, 2001.

Eurostat: International trade in goods – detailed data (DS-018995), https://ec.europa.eu/eurostat/web/international-trade-in-goods/database (last access: 8 August 2025), 2025.

Giostra, U., Furlani, F., Arduini, J., Cava, D., Manning, A. J., O'Doherty, S. J., Reimann, S., and Maione, M.: The determination of a "regional" atmospheric background mixing ratio for anthropogenic greenhouse gases: a comparison of two independent methods, Atmos. Environ., 45, 7396–7405, https://doi.org/10.1016/j.atmosenv.2011.06.076, 2011.

Giovannini, L., Ferrero, E., Karl, T., Rotach, M. W., Staquet, C., Trini Castelli, S., and Zardi, D.: Atmospheric pollutant dispersion over complex terrain: challenges and needs for improving air quality measurements and modeling, Atmosphere, 11, 646, https://doi.org/10.3390/atmos11060646, 2020.

Hanson, M. L., Madronich, S., Solomon, K., Sulbaek Andersen, M. P., and Wallington, T. J.: Trifluoroacetic acid in the environment: consensus, gaps, and next steps, Environ. Toxicol. Chem., 43, 2091–2093, https://doi.org/10.1002/etc.5963, 2024.

Hart, L. A.: Model outputs for "Increasing and Widespread Deposition of Trifluoroacetic Acid from Global Emissions of HFO-1234yf in Mobile-Air Conditioning", Zenodo [data set], https://doi.org/10.5281/zenodo.21458539, 2026.

Hart, L., Hossaini, R., Wild, O., Mazzeo, A., Halsall, C., Hou, X., Wang, Z., Chipperfield, M. P., Arduini, J., Krummel, P. B., Lunder, C. R., Mühle, J., O'Doherty, S., Park, S., Reimann, S., Stanley, K. M., Weiss, R. F., and Young, D.: Growth in production and environmental deposition of trifluoroacetic acid due to long-lived CFC replacements and anesthetics, Geophys. Res. Lett., 53, e2025GL119216, https://doi.org/10.1029/2025GL119216, 2026.

Hartz, W. F., Björnsdotter, M. K., Yeung, L. W. Y., Hodson, A., Thomas, E. R., Humby, J. D., Day, C., Jogsten, I. E., Kärrman, A., and Kallenborn, R.: Levels and distribution profiles of per- and polyfluoroalkyl substances (PFAS) in a high Arctic Svalbard ice core, Sci. Total Environ., 871, 161830, https://doi.org/10.1016/j.scitotenv.2023.161830, 2023.

Held, M., Rosat, N., Georges, G., Pengg, H., and Boulouchos, K.: Lifespans of passenger cars in Europe: empirical modelling of fleet turnover dynamics, Eur. Transp. Res. Rev., 13, 9, https://doi.org/10.1186/s12544-020-00464-0, 2021.

Henne, S., Shallcross, D. E., Reimann, S., Xiao, P., Brunner, D., O'Doherty, S., and Buchmann, B.: Future emissions and atmospheric fate of HFC-1234yf from mobile air conditioners in Europe, Environ. Sci. Technol., 46, 1650–1658, https://doi.org/10.1021/es2034608, 2012.

Henne, S., Storck, F. R., Wöhrnschimmel, H., Leuenberger, M., Vollmer, M. K., and Reimann, S.: Trifluoroacetate (TFA) in precipitation and surface waters in Switzerland: trends, source attribution, and budget, Atmos. Chem. Phys., 25, 18157–18186, https://doi.org/10.5194/acp-25-18157-2025, 2025.

Holland, R., Adam, B., H Khan, M. A., Young, D., O'Doherty, S., Stanley, K. M., Rigby, M., and Shallcross, D. E.: TFA generation and deposition over Europe may currently see a greater influence from HFO-1234yf than HFC-134a, Environ. Sci. Tech. Lett., https://doi.org/10.1021/acs.estlett.6c00356, 2026.

Holland, R., Khan, M. A. H., Driscoll, I., Chhantyal-Pun, R., Derwent, R. G., Taatjes, C. A., Orr-Ewing, A. J., Percival, C. J., and Shallcross, D. E.: Investigation of the production of trifluoroacetic acid from two halocarbons, HFC-134a and HFO-1234yf, and its fates using a global three-dimensional chemical transport model, ACS Earth Space Chem., 5, 849–857, https://doi.org/10.1021/acsearthspacechem.0c00355, 2021.

Hossaini, R., Sherry, D., Wang, Z., Chipperfield, M. P., Feng, W., Oram, D. E., Adcock, K. E., Montzka, S. A., Simpson, I. J., Mazzeo, A., Leeson, A. A., Atlas, E., and Chou, C. C.-K.: On the atmospheric budget of 1,2-dichloroethane and its impact on stratospheric chlorine and ozone (2002–2020), Atmos. Chem. Phys., 24, 13457–13475, https://doi.org/10.5194/acp-24-13457-2024, 2024.

Hou, X., Hossaini, R., Wild, O., Mazzeo, A., Pope, R. J., Wang, Y., Wang, S., Zhao, Y., Lee, J., Zhu, B., Zhao, T., and Pandey, A. K.: Tropospheric OH and its trends: new insight into atmospheric processes and implications for methane lifetime, Atmos. Chem. Phys., 26, 13767–13793, https://doi.org/10.5194/acp-26-13767-2026, 2026.

ICF International: Greenhouse Gas Inventory Improvement Project, https://assets.publishing.service.gov.uk/media/5a78ac58ed915d042206473a/3844-greenhouse-gas-inventory-improvement-project-deve.PDF (last access: 8 May 2026), 2011.

IPCC: 2006 IPCC Guidelines for National Greenhouse Gas Inventories, prepared by the National Greenhouse Gas Inven-

tories Programme, edited by: Eggleston, H. S., Buendia, L., Miwa, K., Ngara, T., and Tanabe, K., IGES, Hayama, Japan, https://www.ipcc-nggip.iges.or.jp/public/2006gl/ (last access: 9 November 2026), 2006.

Jacob, D. J., Logan, J. A., and Murti, P. P.: Effect of rising Asian emissions on surface ozone in the United States, Geophys. Res. Lett., 26, 2175–2178, https://doi.org/10.1029/1999GL900450, 1999.

Joerss, H., Freeling, F., Van Leeuwen, S., Hollender, J., Liu, X., Nödler, K., Wang, Z., Yu, B., Zahn, D., and Sigmund, G.: Pesticides can be a substantial source of trifluoroacetate (TFA) to water resources, Environ. Int., 193, 109061, https://doi.org/10.1016/j.envint.2024.109061, 2024.

Kazil, J., McKeen, S., Kim, S. W., Ahmadov, R., Grell, G. A., Talukdar, R. K., and Ravishankara, A. R.: Deposition and rainwater concentrations of trifluoroacetic acid in the United States from the use of HFO-1234yf, J. Geophys. Res.-Atmos., 119, 14059–14079, https://doi.org/10.1002/2014JD022058, 2014.

Khan, M. A. H., Mendes, D. C., Holland, R. E. T., Garavagno, M. D. L. A., Orr-Ewing, A. J., Stanley, K. M., O'Doherty, S. J., Young, D., Vollmer, M. K., Antony, A. J., Karamshahi, F., Wallington, T. J., Percival, C. J., Bacak, A., Derwent, R. G., and Shallcross, D. E.: Global modeling of trifluoroacetic acid surface concentration and deposition from the gas-phase oxidation of a wide range of precursor hydrofluoroolefins, Environ. Sci.-Atmos., https://doi.org/10.1039/D5EA00108K, 2026.

Killen, B., Fisher, J. A., Hansen, C. S., Krummel, P., Vollmer, M. K., and Kable, S.: Atmospheric fates and global warming potential of HFO-1234ze(E) and its degradation product trifluoroacetaldehyde (CF3CHO), Environ. Sci.-Atmos., https://doi.org/10.1039/D6EA00034G, 2026.

Kish, L.: Survey Sampling, Wiley Classics Library, John Wiley & Sons, New York, USA, ISBN 0-471-10949-5, 1995.

Koffi Lefeivre, B., Dentener, F., Janssens-Maenhout, G., Guizzardi, D., Crippa, M., Diehl, T., Galmarini, S., and Solazzo, E.: Hemispheric Transport of Air Pollution (HTAP): Specification of the HTAP2 experiments – ensuring harmonized modelling, EUR 28255 EN, Publications Office of the European Union, Luxembourg, https://doi.org/10.2788/725244, 2016.

Li, X., Hou, M., Jiang, S., Cousins, I. T., Li, P., Shi, Y., Cai, Y., and Jiang, G.: Atmospheric transport and deposition of PFAS in East Antarctica: evidence from snow transect measurements and a multidecadal record, Sci. Adv., 12, eadz4749, https://doi.org/10.1126/sciadv.adz4749, 2026.

Luecken, D. J., Waterland, R. L., Papasavva, S., Taddonio, K. N., Hutzell, W. T., Rugh, J. P., and Andersen, S. O.: Ozone and TFA impacts in North America from degradation of 2,3,3,3-tetrafluoropropene (HFO-1234yf), a potential greenhouse gas replacement, Environ. Sci. Technol., 44, 343–348, https://doi.org/10.1021/es902481f, 2010.

McGillen, M. R., Fried, Z. T. P., Khan, M. A. H., Kuwata, K. T., Martin, C. M., O'Doherty, S., Pecere, F., Shallcross, D. E., Stanley, K. M., and Zhang, K.: Ozonolysis can produce long-lived greenhouse gases from commercial refrigerants, P. Natl. Acad. Sci. USA, 120, e2312714120, https://doi.org/10.1073/pnas.2312714120, 2023.

Naik, V., Voulgarakis, A., Fiore, A. M., Horowitz, L. W., Lamarque, J.-F., Lin, M., Prather, M. J., Young, P. J., Bergmann, D., Cameron-Smith, P. J., Cionni, I., Collins, W. J., Dalsøren, S. B., Doherty, R., Eyring, V., Faluvegi, G., Folberth, G. A., Josse, B., Lee, Y. H., MacKenzie, I. A., Nagashima, T., van Noije, T. P. C., Plummer, D. A., Righi, M., Rumbold, S. T., Skeie, R., Shindell, D. T., Stevenson, D. S., Strode, S., Sudo, K., Szopa, S., and Zeng, G.: Preindustrial to present-day changes in tropospheric hydroxyl radical and methane lifetime from the Atmospheric Chemistry and Climate Model Intercomparison Project (ACCMIP), Atmos. Chem. Phys., 13, 5277–5298, https://doi.org/10.5194/acp-13-5277-2013, 2013.

Nakamoto, Y., Nishijima, D., and Kagawa, S.: The role of vehicle lifetime extensions of countries on global CO2 emissions, J. Clean. Prod., 207, 1040–1046, https://doi.org/10.1016/j.jclepro.2018.10.054, 2019.

Nawaz, M. O., Henze, D. K., Anenberg, S. C., Braun, C., Miller, J., and Pronk, E.: A source apportionment and emission scenario assessment of PM2.5- and O3-related health impacts in G20 countries, GeoHealth, 7, e2022GH000713, https://doi.org/10.1029/2022GH000713, 2023.

Neale, P. J., Hylander, S., Banaszak, A. T., Häder, D.-P., Rose, K. C., Vione, D., Wängberg, S.-Å., Jansen, M. A. K., Busquets, R., Andersen, M. P. S., Madronich, S., Hanson, M. L., Schikowski, T., Solomon, K. R., Sulzberger, B., Wallington, T. J., Heikkilä, A. M., Pandey, K. K., Andrady, A. L., Bruckman, L. S., White, C. C., Zhu, L., Bernhard, G. H., Bais, A., Aucamp, P. J., Chiodo, G., Cordero, R. R., Petropavlovskikh, I., Neale, R. E., Olsen, C. M., Hales, S., Lal, A., Lingham, G., Rhodes, L. E., Young, A. R., Robson, T. M., Robinson, S. A., Barnes, P. W., Bornman, J. F., Harper, A. B., Lee, H., Calderón, R. M., Ossola, R., Paul, N. D., Revell, L. E., Wang, Q.-W., and Zepp, R. G.: Environmental consequences of interacting effects of changes in stratospheric ozone, ultraviolet radiation, and climate: UNEP Environmental Effects Assessment Panel, update 2024, Photochem. Photobiol. Sci., 24, 357–392, https://doi.org/10.1007/s43630-025-00687-x, 2025.

OECD: Reconciling Terminology of the Universe of Per- and Polyfluoroalkyl Substances: Recommendations and Practical Guidance, OECD Series on Risk Management, No. 61, OECD Publishing, Paris, France, https://doi.org/10.1787/e458e796-en, 2021.

OICA: Motor vehicle production and sales statistics, International Organization of Motor Vehicle Manufacturers, Paris, France, https://oica.net/statistics/ (last access: 29 July 2025), 2025.

Papadimitriou, V. C., Talukdar, R. K., Portmann, R. W., Ravishankara, A. R., and Burkholder, J. B.: CF3CF=CH2 and (Z)-CF3CF=CHF: temperature dependent OH rate coefficients and global warming potentials, Phys. Chem. Chem. Phys., 10, 808–820, https://doi.org/10.1039/b714382f, 2008.

Papasavva, S., Luecken, D.J., Waterland, R.L., Taddonio, K.N. and Andersen, S.O., 2009. Estimated 2017 refrigerant emissions of 2, 3, 3, 3-tetrafluoropropene (HFC-1234yf) in the United States resulting from automobile air conditioning. Environ. Sci. Technol., 43, 9252–9259, https://doi.org/10.1021/es902124u, 2009.

Pérez-Peña, M. P., Fisher, J. A., Hansen, C., and Kable, S. H.: Assessing the atmospheric fate of trifluoroacetaldehyde (CF3CHO) and its potential as a new source of fluoroform (HFC-23) using the AtChem2 box model, Environ. Sci.-Atmos., 3, 1767–1777, https://doi.org/10.1039/D3EA00120B, 2023.

Persaud, D., Joudan, S., VandenBoer, T. C., and Young, C. J.: Atmospheric removal of trifluoroacetic acid by dry and wet depo-

sition: a multiyear analysis in Toronto, Environ. Sci. Tech. Lett., 13, 261–267, https://doi.org/10.1021/acs.estlett.5c01100, 2026.

Pickard, H. M., Criscitiello, A. S., Persaud, D., Spencer, C., Muir, D. C. G., Lehnherr, I., Sharp, M. J., De Silva, A. O., and Young, C. J.: Ice core record of persistent short-chain fluorinated alkyl acids: evidence of the impact from global environmental regulations, Geophys. Res. Lett., 47, e2020GL087535, https://doi.org/10.1029/2020GL087535, 2020.

Prather, M. J., Holmes, C. D., and Hsu, J.: Reactive greenhouse gas scenarios: systematic exploration of uncertainties and the role of atmospheric chemistry, Geophys. Res. Lett., 39, L09803, https://doi.org/10.1029/2012GL051440, 2012.

Raheem, D., Trovò, M., Carmona Mora, C., and Vassent, C.: Persistent organic pollutants' threats and impacts on food safety in the polar regions – a concise review, Pollutants, 5, 14, https://doi.org/10.3390/pollutants5020014, 2025.

Ryan, E. and Wild, O.: Calibrating a global atmospheric chemistry transport model using Gaussian process emulation and ground-level concentrations of ozone and carbon monoxide, Geosci. Model Dev., 14, 5373–5391, https://doi.org/10.5194/gmd-14-5373-2021, 2021.

Salierno, G.: On the chemical pathways influencing the effective global warming potential of commercial hydrofluoroolefin gases, ChemSusChem, 17, e202400280, https://doi.org/10.1002/cssc.202400280, 2024.

Sanz Rodriguez, E., Lai, M., Stevens, H., Nation, M. K., Plummer, C. T., Jong, L. M., Roberts, J. L., Moy, A. D., Bowie, A. R., Curran, M. A., and Paull, B.: Seasonal variation of trifluoroacetic acid (TFA) in Antarctic ice cores analysed by direct injection non-suppressed ion chromatography–mass spectrometry (nsIC-MS), Sci. Total Environ., 988, 179837, https://doi.org/10.1016/j.scitotenv.2025.179837, 2025.

Scheurer, M., Nödler, K., Freeling, F., Janda, J., Happel, O., Riegel, M., Müller, U., Storck, F. R., Fleig, M., Lange, F. T., Brunsch, A., and Brauch, H.-J.: Small, mobile, persistent: trifluoroacetate in the water cycle – overlooked sources, pathways, and consequences for drinking water supply, Water Res., 126, 460–471, https://doi.org/10.1016/j.watres.2017.09.045, 2017.

Shindell, D. T., Chin, M., Dentener, F., Doherty, R. M., Faluvegi, G., Fiore, A. M., Hess, P., Koch, D. M., MacKenzie, I. A., Sanderson, M. G., Schultz, M. G., Schulz, M., Stevenson, D. S., Teich, H., Textor, C., Wild, O., Bergmann, D. J., Bey, I., Bian, H., Cuvelier, C., Duncan, B. N., Folberth, G., Horowitz, L. W., Jonson, J., Kaminski, J. W., Marmer, E., Park, R., Pringle, K. J., Schroeder, S., Szopa, S., Takemura, T., Zeng, G., Keating, T. J., and Zuber, A.: A multi-model assessment of pollution transport to the Arctic, Atmos. Chem. Phys., 8, 5353–5372, https://doi.org/10.5194/acp-8-5353-2008, 2008.

Sindelarova, K., Markova, J., Simpson, D., Huszar, P., Karlicky, J., Darras, S., and Granier, C.: High-resolution biogenic global emission inventory for the time period 2000–2019 for air quality modelling, Earth Syst. Sci. Data, 14, 251–270, https://doi.org/10.5194/essd-14-251-2022, 2022.

Soulie, A., Granier, C., Darras, S., Zilbermann, N., Doumbia, T., Guevara, M., Jalkanen, J.-P., Keita, S., Liousse, C., Crippa, M., Guizzardi, D., Hoesly, R., and Smith, S. J.: Global anthropogenic emissions (CAMS-GLOB-ANT) for the Copernicus Atmosphere Monitoring Service simulations of air quality forecasts and reanalyses, Earth Syst. Sci. Data, 16, 2261–2279, https://doi.org/10.5194/essd-16-2261-2024, 2024.

Stevenson, D. S., Zhao, A., Naik, V., O'Connor, F. M., Tilmes, S., Zeng, G., Murray, L. T., Collins, W. J., Griffiths, P. T., Shim, S., Horowitz, L. W., Sentman, L. T., and Emmons, L.: Trends in global tropospheric hydroxyl radical and methane lifetime since 1850 from AerChemMIP, Atmos. Chem. Phys., 20, 12905–12920, https://doi.org/10.5194/acp-20-12905-2020, 2020.

Strode, S. A., Wang, J. S., Manyin, M., Duncan, B., Hossaini, R., Keller, C. A., Michel, S. E., and White, J. W. C.: Strong sensitivity of the isotopic composition of methane to the plausible range of tropospheric chlorine, Atmos. Chem. Phys., 20, 8405–8419, https://doi.org/10.5194/acp-20-8405-2020, 2020.

Sulbaek Andersen, M. P. and Nielsen, O. J.: Tropospheric photolysis of CF3CHO, Atmos. Environ., 272, 118935, https://doi.org/10.1016/j.atmosenv.2021.118935, 2022.

Sulbaek Andersen, M. P., Wallington, T. J., Burkholder, J. B., Madronich, S., Hanson, M. L., Van Hoomissen, D., and Solomon, K. R.: Yields of perfluorocarboxylic acids from the atmospheric oxidation of Montreal Protocol related gases, Environ. Sci.-Atmos., https://doi.org/10.1039/D5EA00179J, 2026.

TEAP: UNEP: 2022 Report of the Medical and Chemical Technical Options Committee (MCTOC), 2022 Assessment Report, Technology and Economic Assessment Panel, Ozone Secretariat, Nairobi, Kenya, ISBN 978-9966-076-99-1, https://ozone.unep.org/science/assessment/teap (last access: 9 November 2026), 2022.

Thomson, J. D., Campbell, J. S., Edwards, E. B., Medcraft, C., Nauta, K., Pérez-Peña, M. P., Fisher, J. A., Osborn, D. L., Kable, S. H., and Hansen, C. S.: Fluoroform (CHF3) production from CF3CHO photolysis and implications for the decomposition of hydrofluoroolefins and hydrochlorofluoroolefins in the atmosphere, J. Am. Chem. Soc., 147, 33–38, https://doi.org/10.1021/jacs.4c11776, 2025.

UNEP: Fact Sheet 12: Mobile Air-Conditioning, Background Material for HFC Workshop, Bangkok, 20–21 April 2015, https://ozone.unep.org/meetings/workshop-hydrofluorocarbon-management-2015/presession-documents, last access: 24 June 2025, 2015.

UNFCCC: National Inventory Submissions 2025, https://unfccc.int/ghg-inventories-annex-i-parties/2025 (last access: 15 October 2026), 2025.

United States Environmental Protection Agency (US EPA): Global overview of HCFC, HFC, and HFO/HCFO production, https://downloads.regulations.gov/EPA-HQ-OAR-2021-0643-0064/attachment_31.pdf (last access: May 2025), 2022.

van der Werf, G. R., Randerson, J. T., Giglio, L., van Leeuwen, T. T., Chen, Y., Rogers, B. M., Mu, M., van Marle, M. J. E., Morton, D. C., Collatz, G. J., Yokelson, R. J., and Kasibhatla, P. S.: Global fire emissions estimates during 1997–2016, Earth Syst. Sci. Data, 9, 697–720, https://doi.org/10.5194/essd-9-697-2017, 2017.

Van Hoomissen, D., Chattopadhyay, A., Montzka, S. A., and Burkholder, J. B.: CHF3 (HFC-23) and CF3CHO quantum yields in the pulsed laser photolysis of CF3CHO at 248, 266, 281, and 308 nm, ACS Earth Space Chem., 9, 589–602, https://doi.org/10.1021/acsearthspacechem.4c00316, 2025.

Vollmer, M. K., Pitt, J. R., Young, D., Henne, S., Mitrevski, B., Mühle, J., Ganesan, A., Arduini, J., Manning, A. J., Wagenhäuser, T., Redington, A. L., Melo, D. B., Murphy, B., Gluck-

mann, R., Stanley, K. M., Krummel, P. B., Lunder, C. R., Yun, J., Rust, D., Wenger, A., Guillevic, M., Kim, J., Wang, R. H. J., Rhee, T. S., Constantin, L., Frumau, A., Harth, C. M., Salameh, P. K., Hermansen, O., Rigby, M., Western, L. M., Engel, A., O'Doherty, S., Park, S., Maione, M., Fraser, P. J., Prinn, R. G., Weiss, R. F., and Reimann, S.: Global Observations and European emissions of the halogenated olefins HFO-1234yf, HFO-1234ze(E), and HCFO-1233zd(E) from the AGAGE (Advanced Global Atmospheric Gases Experiment) network, Atmos. Chem. Phys., 26, 6993–7012, https://doi.org/10.5194/acp-26-6993-2026, 2026a.

Vollmer, M. K., Pitt, J. R., Young, D., Henne, S., Mitrevski, B., Mühle, J., Ganesan, A., Arduini, J., Manning, A. J., Wagenhäuser, T., Redington, A. L., Melo, D. B., Murphy, B., Gluckmann, R., Stanley, K. M., Krummel, P. B., Lunder, C. R., Yun, J., Rust, D., Wenger, A., Guillevic, M., Kim, J., Wang, R. H. J., Rhee, T. S. Constantin, L., Frumau, A., Harth, C. M., Salameh, P. K., Hermansen, O., Rigby, M., Western, L. M., Engel, A., O'Doherty, S., Park, S., Maione, M., Fraser, P. J., Prinn, R. G., Weiss, R. F., and Reimann, S.: Global Observations and European emissions of the halogenated olefins HFO-1234yf, HFO-1234ze(E), and HCFO-1233zd(E) from the AGAGE (Advanced Global Atmospheric Gases Experiment) network, Zenodo [dataset], https://doi.org/10.5281/zenodo.20020038, 2026.

Wang, Y., Liu, L., Qiao, X., Sun, M., Guo, J., and Zhang, J.: Trifluoroacetic acid (TFA) deposition and accumulation potential from future emissions of HFO-1234yf in China, Environ. Sci. Technol., https://doi.org/10.1021/acs.est.5c18352, 2026.

Wang, Y., Liu, L., Qiao, X., Sun, M., Guo, J., Zhang, J., and Zhao, B.: Projections of national-gridded emissions of hydrofluoroolefins (HFOs) in China, Environ. Sci. Technol., 57, 8650–8659, https://doi.org/10.1021/acs.est.2c09263, 2023.

Wang, Y., Liu, L., Qiao, X., Sun, M., Guo, J., Zhao, B., and Zhang, J.: Atmospheric fate and impacts of HFO-1234yf from mobile air conditioners in East Asia, Sci. Total Environ., 916, 170137, https://doi.org/10.1016/j.scitotenv.2024.170137, 2024.

Warncke, K. and Gschrey, B.: Inventory of F-Gases 2023/2024: Data on H(C)FCs, PFCs, H(C)FE and PFPMIE for national emission reporting under the United Nations Framework Convention on Climate Change for the reporting years 2023 and 2024, TEXTE 74/2026, Umweltbundesamt, Dessau-Roßlau, https://doi.org/10.60810/openumwelt-8227, 2026.

Wild, O. and Akimoto, H.: Intercontinental transport of ozone and its precursors in a three-dimensional global CTM, J. Geophys. Res.-Atmos., 106, 27729–27744, https://doi.org/10.1029/2000JD000123, 2001.

Wild, O., Prather, M. J., Akimoto, H., Sundet, J. K., Isaksen, I. S. A., Crawford, J. H., Davis, D. D., Avery, M. A., Kondo, Y., Sachse, G. W., and Sandholm, S. T.: Chemical transport model ozone simulations for spring 2001 over the western Pacific: regional ozone production and its global impacts, J. Geophys. Res.-Atmos., 109, D15S02, https://doi.org/10.1029/2003JD004041, 2004.

Yang, L. H., Jacob, D. J., Lin, H., Dang, R., Bates, K. H., East, J. D., Travis, K. R., Pendergrass, D. C., and Murray, L. T.: Assessment of hydrogen's climate impact is affected by model OH biases, Geophys. Res. Lett., 52, e2024GL112445, https://doi.org/10.1029/2024GL112445, 2025.